

# Farther the Shift, Sparser the Representation: Analyzing OOD Mechanisms in LLMs

Mingyu Jin<sup>\*</sup>, Yutong Yin<sup>†</sup>, Jingcheng Niu<sup>‡</sup>, Qingcheng Zeng<sup>†</sup>,  
Wujiang Xu<sup>\*</sup>, Mengnan Du<sup>§</sup>, Wei Cheng<sup>¶</sup>, Zhaoran Wang<sup>†</sup>,  
Tianlong Chen<sup>||</sup>, Dimitris N. Metaxas<sup>\*</sup>

## Abstract

In this work, we investigate how Large Language Models (LLMs) adapt their internal representations when encountering inputs of increasing difficulty, quantified as the degree of out-of-distribution (OOD) shift. We reveal a consistent and quantifiable phenomenon: as task difficulty increases, whether through harder reasoning questions, longer contexts, or adding answer choices, the last hidden states of LLMs become substantially sparser. In short, *the farther the shift, the sparser the representations*. This sparsity–difficulty relation is observable across diverse models and domains, suggesting that language models respond to unfamiliar or complex inputs by concentrating computation into specialized subspaces in the last hidden state. Through a series of controlled analyses with a learning dynamic explanation, we demonstrate that this sparsity is not incidental but an adaptive mechanism for stabilizing reasoning under OOD. Leveraging this insight, we design *Sparsity-Guided Curriculum In-Context Learning (SG-ICL)*, a strategy that explicitly uses representation sparsity to schedule few-shot demonstrations, leading to considerable performance enhancements. Our study provides new mechanistic insights into how LLMs internalize OOD challenges. The source code is available at the URL: <https://github.com/MingyuJ666/sparsityLLM>.

## 1 Introduction

Large Language Models (LLMs) act as powerful substrates for reasoning (Wei et al., 2022; Li et al., 2025b) and knowledge-intensive interaction (Wang et al., 2024b; Chen et al., 2023; Team et al., 2025). Yet, their reliability frequently falters when prompts demand deeper inference or deviate from training distributions, leading to sharp performance degradation in out-of-distribution (OOD) regimes (Lightman et al., 2024; Li et al., 2025a). This distinction between memorized competence (in-distribution; ID) and generalized reasoning (OOD) has prompted a shift from behavioral metrics to internal investigation via mechanistic interpretability (Qi et al., 2025; Wang et al., 2025a).

Currently, research split between a *mechanistic* perspective that maps behavior to specific circuits (Wang et al., 2022; Conmy et al., 2023) and a *statistical* view that analyzes the geometry of distributed representations

---

<sup>\*</sup>Rutgers University

<sup>†</sup>Northwestern University

<sup>‡</sup>UKP Lab, TU Darmstadt

<sup>§</sup>New Jersey Institute of Technology

<sup>¶</sup>NEC Lab American

<sup>||</sup>University of North Carolina at Chapel Hill

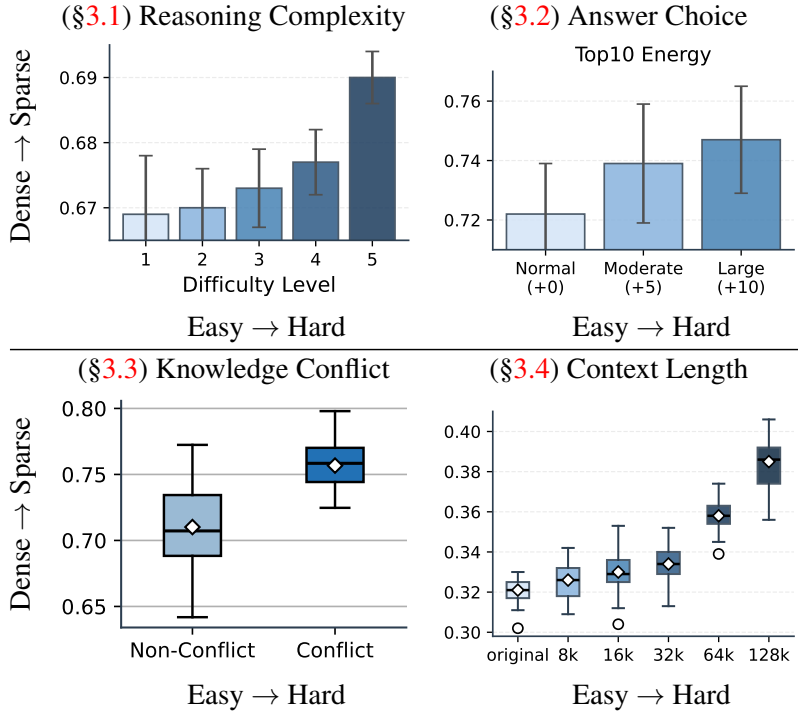


Figure 1: **Harder Inputs Induce Sparser Representations.** Across all four controlled difficulty axes, the last hidden states become progressively sparser as tasks get harder. Results are shown for **Qwen2.5-3B** using Top-10% Energy; nevertheless, the same trend holds across difficulty settings, sparsity metrics, and LLM sizes.

(Hewitt and Manning, 2019; Heinzerling and Inui, 2024). What remains significantly less explored is whether the transition from mastered ID performance to the uncertain OOD frontier is governed by a consistent representational signature.

*How Representation adapts when language models face harder reasoning questions?*

We identify *sparsity*, the property where a high-dimensional representation is dominated by a small subset of active units, as a promising candidate for this signal. While sparsity is a pervasive phenomenon extensively discussed as evidence for specialization or modularity (Olshausen and Field, 1996; Glorot et al., 2011; Frankle and Carbin, 2019; Xiong et al., 2025, *inter alia*), and has been examined in LLMs regarding intrinsic dimensionality (Aghajanyan et al., 2021; De Cao et al., 2022). However, most interpretability work treats sparsity as a largely static background property Liu et al. (2025), rather than as an explanatory variable that changes systematically with task conditions and can therefore explain differences in behavior.

In this work, we make progress on these questions by uncovering a robust connection between representational sparsity and task difficulty. Concretely, when a language model is prompted with a task, *as task difficulty increases, the model’s representations become systematically sparser.*

We quantify *sparsity* in the *last hidden state* using the  $\ell_1$  Norm and Top- $k$  Energy (for multiple  $k$ ), and operationalize *difficulty* by controlled increases in OOD shift across diverse reasoning tasks (reasoning complexity, number of answer choices, conflicting knowledge, and context length; §3.1–§3.4; summarizes in Figure 1). Across all settings, harder inputs consistently yield sparser last-layer representations, and this trend holds across tasks, sparsity metrics, and model families, suggesting a systematic aspect of LLM inference

rather than an incidental artifact. In practical terms, increased sparsity means that fewer representation dimensions carry most of the activation mass, implying that harder prompts drive the model to rely on a more concentrated set of features. This observation bridges representational and mechanistic perspectives, motivating us to probe which internal pathways or features dominate as difficulty increases.

This positions sparsity as a candidate organizing principle for studying how internal computation adapts under increased reasoning demands in the language model.

Finally, we show that the sparsity-difficulty connection is actionable. By treating sparsity as a practical signal of task complexity, we design a *sparsity-guided curriculum* strategy that selects in-context demonstrations whose difficulty aligns with the query. This principle yields consistent improvements in few-shot reasoning, establishing sparsity not only as an analysis tool but also as a lever for improving model reasoning performance.

To systematically address these gaps, we organize our study around three core research questions:

- **RQ1:** How does the geometry of the last hidden state evolve as reasoning tasks become increasingly difficult?
- **RQ2:** What mechanisms drive the emergence of sparsity when models face OOD challenges?
- **RQ3:** How can this sparsity signal be practically leveraged to enhance model reasoning capabilities?

Guided by these questions, our primary findings are summarized as follows:

❶ **Sparsity increases with difficulty in a robust and controlled manner.** We uncover a consistent relationship where last hidden state activations become sparser as question difficulty increases, across multiple reasoning benchmarks including MATH500 (Lightman et al., 2024) and LongReason (Li et al., 2025a). To enable precise control over difficulty, we introduce *MMLU-Robust*, a benchmark that induces graded difficulty via controlled distractor augmentation.

❷ **Learning dynamics connect density to familiarity.** We identify a fundamental link between representation density and data familiarity. Our analysis suggests that high activation density is a learned attribute: as models master training data, they consolidate representations. Importantly, this trend already emerges during *pretraining*, without any task-specific fine-tuning, suggesting it is a general property of learned representations rather than a downstream artifact. Conversely, sparsity serves as the intrinsic default state for harder or less familiar inputs. We also provide a *theoretical derivation* to explain the learning dynamic U-Shape curve.

❸ **Sparsity-guided curricula improve reasoning.** By validating sparsity as a reliable proxy for difficulty, we propose Sparsity-Guided Curriculum In-Context Learning (SG-ICL). Unlike standard strategies that select demonstrations based solely on semantic similarity, SG-ICL introduces a difficulty-aware selection mechanism. This approach yields substantial gains; for instance, SG-ICL achieves 76.60% accuracy on MATH500 with Qwen2.5-7B, surpassing the strong Auto-CoT baseline (75.20%).

## 2 Preliminaries

★ **Experimental Setup** We conduct all experiments under the *Implicit Reasoning setting*. Although Chain-of-Thought (CoT; Wei et al., 2022) prompting also produces observable sparsity patterns, its effects are

noticeably less stable. In contrast, the Implicit reasoning setup yields clearer and more consistent activation dynamics, allowing us to present more interpretable visualizations. The prompt we use can be found in the Appendix A.3. We focus primarily on the *last hidden state* for the same reason. Although related sparsity trends are also present in intermediate layers, they are typically weaker and less consistent across tasks and models. By contrast, the final layer exhibits the clearest and most stable pattern, making it the most interpretable layer for our analysis.

**★ Last Hidden State** We consider a transformer-based LM  $f_\theta(\cdot)$  with  $L$  stacked decoder layers, where each layer  $\ell$  consists of a multi-head self-attention ( $\text{Attn}^{(\ell)}(\cdot)$ ) block and a feed-forward network ( $\text{MLP}^{(\ell)}(\cdot)$ ). For an input token sequence  $x = (x_1, x_2, \dots, x_T)$ , we denote the hidden representation of token  $x_t$  at layer  $\ell$  as  $h_t^{(\ell)} \in \mathbb{R}^d$ , where  $d$  is the hidden dimension. Each layer maintains a residual connection, and its output is computed as:

$$h_t^{(\ell+1)} = \overbrace{h_t^{(\ell)} + \text{Attn}^{(\ell)}(h_t^{(\ell)})}^{h_{\text{mid}}} + \text{MLP}^{(\ell)}(h_{\text{mid}}). \quad (2.1)$$

We focus on the output of each layer in the residual stream, which stores contextualized information aggregated across all tokens in the input prompt. Formally, we use the representation at the final layer of the final input token:

$$h_T^{(L)} = f_\theta^{(L)}(x_{1:T})[-1], \quad (2.2)$$

which we refer to as the *last hidden state*. This representation serves as the latent state used for next-token prediction and downstream tasks.

**★ Sparsity** Prior work has shown that neural networks often exhibit sparsity in their representations or effective parameterization. For example, fine-tuning can occur in low-dimensional subspaces (Aghajanyan et al., 2021), motivating adaptation methods such as LoRA (Hu et al., 2022). In this work, we study the *representational sparsity* of the last hidden state, defined as the extent to which only a small subset of units exhibits large activations. We measure sparsity using several metrics.

First, we compute a normalized  $\ell_1$  magnitude of the last-hidden-state vector:

$$S_{L_1} = \frac{1}{d} \sum_{i=1}^d |h_i|, \quad (2.3)$$

where  $h_i$  denotes the  $i$ -th coordinate of  $h_T^{(L)}$  and  $d$  is the hidden dimension. Lower  $S_{L_1}$  indicates higher sparsity.

Second, we measure the concentration of activation energy using the Top- $k$  Energy:

$$S_{\text{Top-}k} = \sum_{i \in \text{Top-}k\%} h_i^2 / \sum_{i=1}^d h_i^2. \quad (2.4)$$

This metric quantifies the proportion of total activation energy captured by the largest  $k\%$  components. Higher values indicate stronger concentration and thus greater sparsity. Additional metrics, including Hoyer Sparsity and Effective Rank, are reported in Appendix A.2.

**★ Difficulty and OOD** While the term difficulty or OOD is often loosely used in the context of LLMs (Koh et al., 2021), we adopt a more controlled and quantitative view. Given the vast and often opaque nature of LLM pretraining data, strict OOD boundaries are difficult to define. Instead, we operationalize OOD as a spectrum of distributional shift, constructing samples designed to deviate significantly from normal

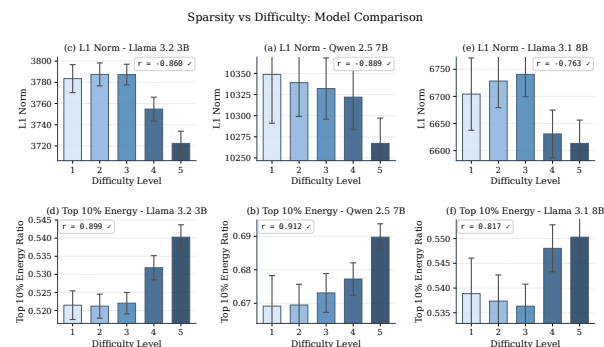
training patterns along four interpretable dimensions: (1) **Task difficulty**: reasoning instances that require deeper or multi-step inference, such as higher-difficulty levels in benchmark datasets (e.g., MATH-500 and DeepMATH-103K has several difficulty levels); (2) **Distractor interference**: problems containing more irrelevant or misleading information, analogous to multiple-choice items with a larger number of distractors; (3) **Knowledge conflict**: prompts that introduce mutually inconsistent facts or constraints, requiring the model to detect and resolve contradictions rather than rely on the prompt; and (4) **Contextual length**: inputs with longer or more compositional contexts.

### 3 RQ1: How does the geometry of the last hidden state evolve as reasoning tasks become increasingly difficult?

In this section, we present results addressing our first research question: *How do last hidden states behave when models encounter hard questions?* We measure sparsity metrics across tasks with varying levels of difficulty along four dimensions: reasoning complexity (§3.1), answer choice expansion (§3.2), knowledge conflict (§3.3), and context length (§3.4). **Spoiler alert**: across all four settings, we observe the same consistent pattern: the harder the task, the sparser the last hidden state.

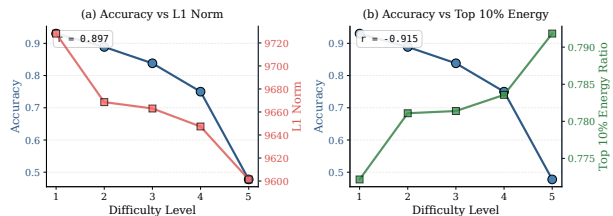
#### 3.1 Sparsity vs Reasoning Complexity

MATH-500 is a subset of (Hendrycks et al., 2021) MATH dataset that contains explicit difficulty annotations. Our initial analysis tests whether representation sparsity correlates with problem difficulty within this graded benchmark. MATH-500 contains 500 mathematical problems spanning five difficulty levels, from basic arithmetic (Level 1) to advanced competition mathematics (Level 5). We evaluate three LLMs (Touvron et al., 2023; Yang et al., 2024): Qwen2.5-7B, Llama3.2-3B, and Llama3.1-8B, and compute sparsity metrics from their last hidden state. As shown in Figure 2a, all models display a consistent monotonic trend: the  $L1$  norm decreases as difficulty increases; the Top-10% Energy Ratio rises, suggesting that the small subset increasingly dominates the activation.



(a) **Sparsity Differences under Different Difficulty Levels.** Last Hidden State sparsity metrics across five difficulty levels and three different models in MATH-500.

**The Strong correlation between LLMs' accuracy and Last Hidden State sparsity ( $\ell_1$  Norm and Top10% Energy).**  
Accuracy vs Sparsity: Qwen 2.5 7B on MATH-500



**Versus sparsity metrics for Qwen2.5-7B on the MATH-500 dataset.**

(b) **Accuracy–Sparsity Correlation.** Sparsity strongly correlates with accuracy ( $L1$ :  $r=0.897$ ; Top-10% Energy:  $r=-0.915$ ).

Figure 2: **Overview of Sparsity Analysis.** Together, the two subfigures paint a consistent picture: Figure 2a (left) shows that difficulty increases sparsity, while Figure 2b (right) shows that sparsity tracks accuracy degradation.

To further validate this connection between reasoning difficulty and sparsity, we examine how sparsity correlates with task performance. As illustrated in Figure 2b, both sparsity metrics exhibit strong negative correlations with accuracy. When problems become harder, accuracy drops sharply, while the  $\ell_1$  Norm decreases and the Top-10% Energy Ratio increases. Together, Figure 2a and Figure 2b paint a consistent picture. Figure 2a demonstrates that higher reasoning difficulty systematically induces stronger sparsity, while Figure 2b shows that increased sparsity is tightly coupled with accuracy degradation. Taken together, these findings establish a coherent causal chain: as tasks become harder, models’ last hidden state exhibits sharper activation compression.

### 3.2 Sparsity vs Answer Choice Expansion

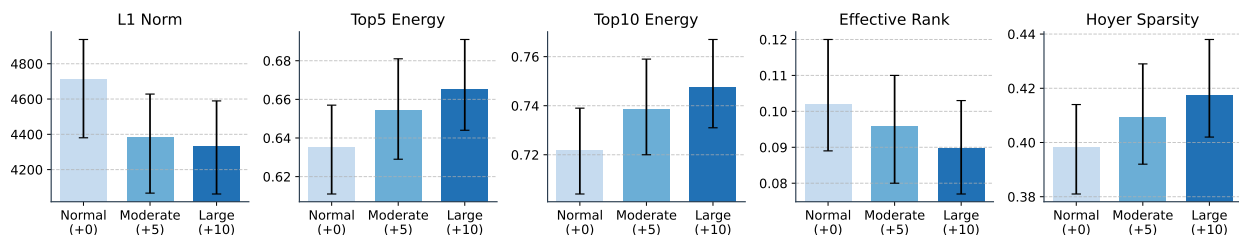


Figure 3: **Sparsity Metrics under Answer Choice Expansion.** Bar plots show mean sparsity across 14 disciplines for five metrics under Normal (+0), Moderate Expansion (+5), and Large Expansion (+10) on Qwen2.5-3B. Error bars indicate the minimum and maximum across disciplines. Increasing task difficulty leads to higher sparsity.

In this setting, we add plausible but incorrect distractor options to multiple-choice questions presented to the LLM. This makes the task strictly harder *ceteris paribus*, as the question content remains unchanged. We obtain different difficulty levels by adding different numbers of distractors. The setup remains simple and controlled, allowing us to study difficulty without confounding textual variation and to isolate OOD behavior.

Particularly, we use MMLU-Pro (Wang et al., 2024c), a multi-domain multiple-choice benchmark covering 14 academic disciplines. The original dataset provides ten answer options, which we use as the baseline **Normal** (+0) configuration. We introduce two additional difficulty levels via answer choice expansion: **Moderate Expansion** (+5), which adds five high-quality, plausible distractors (15 options total), and **Large Expansion** (+10), which adds ten distractors (20 options total). This manipulation increases task difficulty by expanding the solution space while leaving the question content unchanged, providing a controlled way to probe OOD behavior. Using this setup, we construct  $\star$  **MMLU-Robust**, a three-tier extension of MMLU-Pro with Normal (+0), Moderate (+5), and Large (+10) configurations for robustness evaluation. See Appendix A.5 for details.

Figure 3 presents the experiment results, confirming increased sparsity of final-layer hidden states when the tasks become more difficult. We analyzed five key sparsity metrics across all 14 academic areas in MMLU-Pro:  $\ell_1$  Norm, Top-5% Energy, Top-10% Energy, Effective Rank, and Hoyer Sparsity. Across virtually all academic disciplines and for all five sparsity metrics, we observe a *consistent, monotonic trend*: as the question difficulty increases by adding distractors (moving from Normal (+0)  $\rightarrow$  Moderate (+5)  $\rightarrow$  Large (+10)), the last hidden state exhibits higher sparsity. A detailed per-discipline breakdown, along with results for additional models, is provided in Appendix A.5.2, confirming the same trends.

### 3.3 Sparsity vs Knowledge Conflict

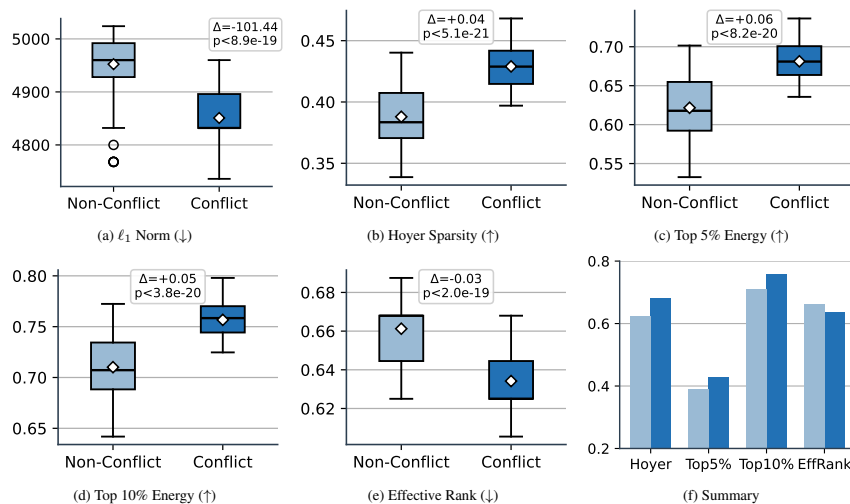
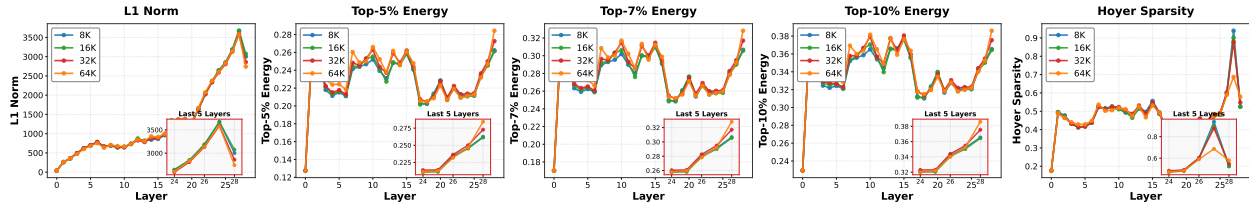


Figure 4: **Sparsity Differences under Knowledge Conflict.** We measure the last hidden state sparsity for two conditions (*non-conflict* (■) and *conflict* (■)) across five metrics for **Qwen2.5-3B**. All results are statistically significant. Arrows denote how each metric relates to sparsity (↑: higher is sparser; ↓: lower is sparser). Again, the harder *conflict* (■) condition is consistently sparser than the *non-conflict* (■) condition across all metrics.

Moreover, we use (Wang et al., 2024b) knowledge conflict dataset to further validate our hypothesis, which labels samples as *conflict* or *non-conflict* by pairing each question with either a truthful or a counterfactual context. In conflict scenarios, the provided context contradicts the model’s parametric knowledge. We think Conflict Knowledge forcing the model to rethink the knowledge sources is a kind of out-of-distribution task. As shown in Figure 4, conflict cases consistently exhibit higher sparsity across all metrics: Specifically, the Hoyer Sparsity (b), Top 5% Energy (c), and Top 10% Energy (d) metrics, where higher values indicate greater sparsity, all show a statistically significant increase for the *Conflict* group compared to the *Non-Conflict* group ( $\Delta \approx +0.0378, +0.0114, \text{ and } +0.0102$  respectively). These differences are **statistically significant**, as confirmed by a paired (Student, 1908) t-test, with all  $p$ -values  $< 2.0 \times 10^{-29}$ . The Summary bar chart (f) synthesizes these findings, clearly illustrating that the latent last hidden representations for conflict instances are generally more compressed and concentrated on fewer dimensions. We provide additional analyses across more LLM families, more model sizes, and more knowledge conflict settings (e.g., the related *distraction* phenomenon; (Niu et al., 2025)) in Appendix A.4.

### 3.4 Sparsity vs Long Context Reasoning

For the long-context reasoning setting, as shown in Figure 5, we use LongReason Li et al. (2025a). This long context dataset offers controllable context lengths and incorporates diverse, realistic reasoning tasks. By analyzing the Last Hidden States across these controlled length variations, we discovered that the sparsity of the hidden states decreases as the input text length increases, as Figure 5. This finding further supports our hypothesis that increasing task difficulty consistently drives the model towards a state of sharper activation compression in the last hidden state. In fact, the sparsity phenomenon induced by OOD shifts is primarily a **terminal behavior**. While intermediate representations remain relatively stable, the decisive shift in activation



CONTEXT: Sparsity metrics across all layers for Qwen2.5-1.5B under varying context lengths (8K, 16K, 32K, 64K).

Figure 5: **Layer-wise Sparsity across Context Lengths.** While intermediate layers show minimal variation across contexts, the final layers exhibit sharp divergence: longer contexts consistently produce sparser representations. This experiment was done at LongReasonQA (Li et al., 2025a), which can control the background context length.

density, which separates OOD from ID, exclusively emerges in the final layer. We provide additional analyses in Appendix A.6.

## 4 RQ2: What mechanisms drive the emergence of sparsity when models face OOD challenges?

Now, we attempt to answer how the sparsity–OOD connection develops during pre-training by training a toy-sized LM from scratch on synthetic data. In this section, we first describe the construction of the synthetic pre-training dataset (§4.1), then analyze the pre-training results (§4.2), and finally connect these dynamics to the emergence of the sparsity–OOD relationship through a combined empirical and theoretical account (§4.3).

### 4.1 Controlled Environment

We create a synthetic knowledge graph dataset that allows precise control over reasoning difficulty and OOD level. The setting is inspired by (Wang et al., 2024a, 2025b; Yin and Wang, 2025; Ye et al., 2025), but we focus on sparsity–difficulty patterns in this controlled symbolic environment rather than the emergence of implicit reasoning.

■ *We validate this mechanism by analyzing representations during pretraining.* Even without task-specific fine-tuning, models pretrained solely on next-token prediction exhibit the same sparsity–difficulty pattern, confirming that this is a fundamental property of the language model.

Specifically, instead of relying on real-world knowledge graphs (where structural and semantic factors are entangled), we generate an artificial graph governed by a set of logical rules. Each rule defines how relations can be composed, e.g.,

$$r_3(x, z) \Leftarrow r_1(x, y) \wedge r_2(y, z), \tag{4.1}$$

ensuring that the resulting graph encodes multi-hop reasoning dependencies. Based on these rules, we construct the dataset in a three-stage process:

**Preliminaries.** We define a Knowledge Graph (KG) as  $\mathcal{G} = (\mathcal{E}, \mathcal{R}, \mathcal{T})$ , where  $\mathcal{E}$  and  $\mathcal{R}$  denote the sets of entities and relations, respectively.  $\mathcal{T} = \{(h, r, t) \mid h, t \in \mathcal{E}, r \in \mathcal{R}\}$  represents the set of facts (triples). The problem difficulty is controlled by logical rules of varying lengths  $L$ .

Model	Params	Steps	Accuracy (% , $\uparrow$ )			$\ell_1$ Norm ( $\downarrow$ )			Top-5 Energy (% , $\uparrow$ )			Top-10 Energy (% , $\uparrow$ )			Eff. Rank ( $\downarrow$ )		
			$\mathcal{D}_{\text{mem}}$	$\mathcal{D}_{\text{ID}}$	$\mathcal{D}_{\text{OOD}}$	$\mathcal{D}_{\text{mem}}$	$\mathcal{D}_{\text{ID}}$	$\mathcal{D}_{\text{OOD}}$	$\mathcal{D}_{\text{mem}}$	$\mathcal{D}_{\text{ID}}$	$\mathcal{D}_{\text{OOD}}$	$\mathcal{D}_{\text{mem}}$	$\mathcal{D}_{\text{ID}}$	$\mathcal{D}_{\text{OOD}}$	$\mathcal{D}_{\text{mem}}$	$\mathcal{D}_{\text{ID}}$	$\mathcal{D}_{\text{OOD}}$
Trans-8-8	0.02B	2500	64.00	42.00	31.00	413.49	413.80	412.79	26.11	26.03	26.26	42.12	42.00	42.34	0.502	0.504	0.500
Trans-16-8	0.04B	2000	71.00	50.00	24.00	413.38	413.30	413.04	25.96	25.94	26.06	41.98	41.98	42.15	0.503	0.503	0.501
Trans-16-16	0.17B	2000	85.00	56.00	44.00	817.60	817.80	816.93	27.70	27.70	27.78	43.70	43.66	43.76	0.483	0.484	0.482
		2500	81.00	58.00	37.00	817.94	818.23	817.20	27.64	27.58	27.76	43.56	43.52	43.69	0.484	0.485	0.483
Trans-32-32	1.34B	1500	78.00	57.00	37.00	1608.10	1604.80	1601.68	30.28	30.54	30.84	46.44	46.72	47.04	0.454	0.451	0.448
		2000	83.00	63.00	34.00	1611.36	1608.21	1605.29	30.00	30.23	30.55	46.11	46.39	46.70	0.458	0.455	0.452
		2500	81.00	63.00	38.00	1616.11	1613.95	1610.50	29.60	29.75	30.11	45.67	45.86	46.22	0.463	0.461	0.457

Table 1: **Emergence of the Sparsity Phenomenon.** We report metrics across 3 levels. The **gradient blue shading**, observed uniquely in **Trans-32-32**, illustrates that the “harder-is-sparsier” mechanism is a learned behavior.

❶ **Graph Construction.** We construct the controlled knowledge graph  $\mathcal{G}$  through a systematic generation pipeline. We first initialize the vocabulary of entities  $\mathcal{E} = \{e_1, \dots, e_N\}$  and relations  $\mathcal{R} = \{P_1, \dots, P_N\}$ , along with a set of  $K$  randomly sampled acyclic logic rules (lengths  $L \in [L_{\min}, L_{\max}]$ ). The graph is seeded with random *atomic triples* (explicit facts). Subsequently, we exhaustively apply the logic rules to these atomic triples to infer all possible *deductible triples* (implicit facts). This process yields a dual-structure graph containing both direct observations and edges logically entailed by reasoning chains.

❷ **Sequence Serialization.** To adapt the structured graph data for a language model, we linearize each triple  $(h, r, t) \in \mathcal{T}$  into a token sequence (e.g., “ $e_1 P_5 e_2$ ”). The model is trained using the standard auto-regressive objective to predict the tail entity  $t$  given the head  $h$  and relation  $r$ .

❸ **Controlled Data Splitting.** To distinguish between rote memorization and logical generalization, we employ a rigorous data splitting strategy. Specifically, we partition the triples  $\mathcal{T}$  into a training set  $\mathcal{D}_{\text{train}}$  and three distinct evaluation subsets:  $\mathcal{D}_{\text{mem}}$  for assessing rote memorization,  $\mathcal{D}_{\text{ID}}$  for testing in-distribution rule composition, and  $\mathcal{D}_{\text{hard}}$  for probing out-of-distribution robustness.

Appendix A.7 provides additional details on the synthetic data construction and the experimental setup used for pre-training the toy-sized LM.

## 4.2 Pretraining Result

We use **Trans- $L$ - $H$**  to denote a Transformer with  $L$  layers and  $H$  attention heads (e.g., Trans-8-8 has 8 layers and 8 heads). We report Accuracy,  $\ell_1$  Norm, Top-5/10 Energy, and Effective Rank across three difficulty levels: Easy/Medium/Hard, which correspond to  $\mathcal{D}_{\text{mem}}$ ,  $\mathcal{D}_{\text{ID}}$ ,  $\mathcal{D}_{\text{hard}}$  respectively. The findings highlight a clear correlation between model scale, training steps, and the emergence of sparsity. These results demonstrate that the relationship between task difficulty and sparsity is a learned phenomenon: it becomes consistent only once the model exits underfitting and reaches sufficient training convergence and capacity. The absence of a clear trend in smaller models may be attributed to the high data complexity relative to their limited capacity. We provide a detailed discussion on the graph data complexity in Appendix A.7.

We make a **fundamental observation** about inference-time representation geometry: the previously reported “harder-is-sparsier” effect is *not only confirmed to instruction-tuned modern LLMs*, but also arises in *standard pretrained Transformer models*, where it emerges as a pretraining-level property. In particular,

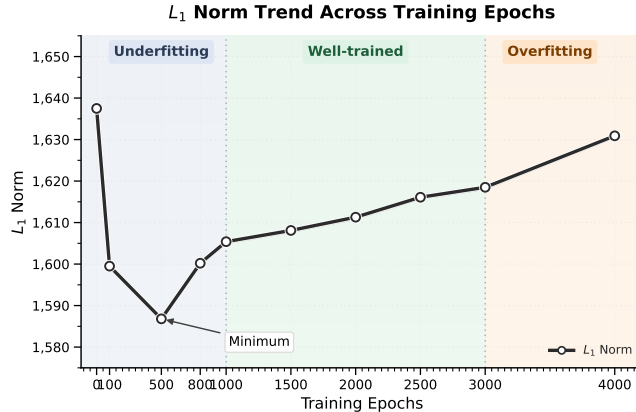


Figure 6: **Learning dynamics via  $\ell_1$  Norm.** The trajectory reveals a two-stage mechanism: initial *feature pruning* (0–500 epochs) followed by *feature consolidation* (green region), where the norm rises as the model learns a more distributed and robust representation.

the “harder-is-sparser” pattern emerges only once the model reaches sufficient capacity and is adequately converged (Table 1).

### 4.3 Learning Dynamics: Sparsity as an Adaptive Representation Mechanism

Nevertheless, Table 1 reveals a counterintuitive phenomenon regarding the temporal evolution of sparsity. Focusing on the **Trans-32-32** model, we observe a monotonic increase in the  $\ell_1$  Norm across training steps (1608.10  $\rightarrow$  1611.36  $\rightarrow$  1616.11 on the Easy set), while accuracy stabilizes. This trend indicates that as training progresses within a healthy regime (avoiding both underfitting and overfitting), the model gradually becomes *less sparse* for the same question.

As illustrated in Figure 6, the training process exhibits a distinct two-phase dynamic.

**Phase I: Feature Selection (0–500 Epochs).** Initially, the  $\ell_1$  Norm drops sharply, indicating a rapid increase in sparsity. In this phase, the model learns to discard noise, pruning irrelevant neurons to identify a core set of discriminative features.

**Phase II: Feature Consolidation (Green Region).** After this initial pruning, the  $\ell_1$  Norm begins a steady ascent (1586.64  $\rightarrow$  1618.52). Crucially, this rise does not imply a return to noise; rather, it signals *representation maturation*. Instead of relying on a few sharp, unstable activations, the model learns to distribute information more evenly across its active neurons. This “smoothing” process creates a more robust representation manifold, allowing the model to generalize better by avoiding over-reliance on single, brittle features.

We give a **theoretical justification** for the emergence of a U-shaped learning dynamic in  $\ell_1$  Norm using a simplified cross-entropy + weight-decay model with kernelized representation dynamics in Section 4.4. We explain this as a shift from early weight decay driven feature contraction (weak head lowers normalized  $\ell_1$ ) to later gradient-aligned amplification on persistently hard examples.

Therefore, high activation density emerges as a *learned privilege* of data familiarity. Since the language model consolidates representations specifically for patterns it has mastered, it maintains high activation density (non-sparsity) in the last hidden state when facing in-distribution samples.

So, difficult or OOD inputs effectively represent the “unseen.” Lacking the familiarity engage the distributed manifolds, the model fails to sustain high-density activations and reverts to a sparse state. This mechanism fundamentally explains our finding: *Farther the Shift, Sparser the Representation*.

#### 4.4 A finite-horizon U-shape certificate for the normalized $\ell_1$ statistic

In [Figure 6](#), we observe a robust U-shape behavior of the representation sparsity during learning: the normalized  $\ell_1$  magnitude of the last hidden state decreases early (*sparsification*), and later increases over another period (*densification*). This appendix provides a finite-horizon theoretical justification on a simplified learning task. Informally, the mechanism is: (i) early training is dominated by weight decay acting on a weak/near-zero head, which contracts feature magnitudes and thus decreases the normalized  $\ell_1$  statistic; (ii) if at some later time the features are already sparse enough but a nontrivial subset of examples remains persistently hard, then the loss gradient aligns with the active coordinates and dominates the contraction over a finite window, forcing the statistic to increase.

##### 4.4.1 Simplified setting: data, model, objectives and gradients

We fix a training set  $\{(x_i, y_i)\}_{i=1}^n$  with labels  $y_i \in \{1, \dots, C\}$ . Let  $\theta(t)$  denote the parameters that generate the last-layer representation, and define

$$h_i(t) := h(x_i; \theta(t)) \in \mathbb{R}^d, \quad i = 1, \dots, n,$$

(e.g., the last hidden state  $h_T^{(L)}$  in the main text, evaluated on the final token of  $x_i$ ). Let  $W(t) \in \mathbb{R}^{C \times d}$  denote the linear readout with rows  $W_c(t) \in \mathbb{R}^d$ . We express the output logits  $z_i(t) \in \mathbb{R}^C$  by

$$z_i(t) := W(t) h_i(t), \quad z_{i,c}(t) = \langle W_c(t), h_i(t) \rangle.$$

Let  $p_i(t) \in \Delta^{C-1}$  be the softmax probabilities:

$$(p_i(t))_c := \frac{e^{z_{i,c}(t)}}{\sum_{c'=1}^C e^{z_{i,c'}(t)}},$$

and let  $e_{y_i} \in \mathbb{R}^C$  be the one-hot vector for label  $y_i$ .

**Training objective (cross-entropy with parameter weight decay).** Define the per-example cross-entropy loss

$$\ell_i(t) := \ell_{\text{ce}}(z_i(t), y_i) = -\log((p_i(t))_{y_i}),$$

and the dataset-averaged cross-entropy

$$\mathcal{L}_{\text{ce}}(\theta, W) := \frac{1}{n} \sum_{i=1}^n \ell_i(t).$$

We regularize the *parameters* that generate the representation (and optionally the readout) via  $\ell_2$  weight decay:

$$\mathcal{L}(\theta, W) := \mathcal{L}_{\text{ce}}(\theta, W) + \frac{\lambda_h}{2} \|\theta\|_2^2 + \frac{\lambda_W}{2} \|W\|_F^2,$$

where  $\lambda_h \geq 0$  is the decay coefficient for  $\theta$  and  $\lambda_W \geq 0$  is optional readout decay. In the analysis below, the effect of weight decay on  $\theta$  is modeled at the feature level as a contraction term  $-\lambda_h h_i(t)$  (plus a residual), captured by the induced dynamics in [\(4.3\)](#).

**Per-example representation gradient.** Define the gradient of  $\ell_i(t)$  with respect to the representation:

$$g_i(t) := \nabla_{h_i} \ell_i(t) = W(t)^\top (p_i(t) - e_{y_i}) \in \mathbb{R}^d.$$

Since  $\|p_i(t) - e_{y_i}\|_2 \leq \sqrt{2}$ , we have

$$\|g_i(t)\|_2 \leq \sqrt{2} \|W(t)\|_{2 \rightarrow 2}, \quad (4.2)$$

where  $\|\cdot\|_{2 \rightarrow 2}$  denotes the operator (spectral) norm.

#### 4.4.2 Induced (kernelized) representation dynamics with weight decay

Let  $K(t) \in \mathbb{R}^{n \times n}$  be a symmetric matrix (a “kernel”) with entries  $K_{ik}(t)$ . We assume the induced dynamics of  $h_i(t) = h(x_i; \theta(t))$  has the form

$$\dot{h}_i(t) = -\frac{1}{n} \sum_{k=1}^n K_{ik}(t) g_k(t) - \lambda_h h_i(t) + r_i(t), \quad (4.3)$$

where  $\lambda_h \geq 0$  is the (effective) feature weight decay coefficient and  $r_i(t)$  is a residual term (e.g., due to non-frozen lower layers), assumed bounded on the horizons of interest.

**Remark 4.1** (A simple setting where (4.3) holds exactly). Consider a frozen backbone feature map  $\phi : \mathcal{X} \rightarrow \mathbb{R}^m$  and a trainable linear representation head  $V(t) \in \mathbb{R}^{d \times m}$  such that

$$\begin{aligned} \theta(t) &\equiv V(t), \\ h_i(t) &= h(x_i; \theta(t)) = V(t)\phi(x_i) =: V(t)\phi_i. \end{aligned}$$

Let the logits be  $z_i(t) = W(t)h_i(t)$  and define  $\ell_i(t) = \ell_{\text{ce}}(z_i(t), y_i)$  as above. If we train  $V$  by gradient flow on  $\mathcal{L}_{\text{ce}}(V, W)$  with  $\ell_2$  weight decay  $\frac{\lambda_h}{2} \|V\|_F^2$  (while  $W$  may also be trained), then a direct chain-rule computation gives

$$\dot{V}(t) = -\frac{1}{n} \sum_{k=1}^n g_k(t) \phi_k^\top - \lambda_h V(t),$$

which leads to

$$\dot{h}_i(t) = \dot{V}(t)\phi_i = -\frac{1}{n} \sum_{k=1}^n \langle \phi_i, \phi_k \rangle g_k(t) - \lambda_h h_i(t).$$

Therefore (4.3) holds with the (time-independent) kernel  $K_{ik} = \langle \phi_i, \phi_k \rangle$  and residual  $r_i(t) \equiv 0$ .

#### 4.4.3 Normalized $\ell_1$ sparsity and a smooth proxy

Recall the normalized  $\ell_1$  statistic (main text):

$$S_{L_1}(h) = \frac{1}{d} \sum_{j=1}^d |h_j|.$$

To obtain a differentiable drift identity, we introduce a smoothed proxy.

**Smoothed primitives.** Fix  $\varepsilon > 0$  and define, for  $u \in \mathbb{R}$ ,

$$\rho_\varepsilon(u) := \sqrt{u^2 + \varepsilon^2}, \quad \psi_\varepsilon(u) := \frac{u}{\sqrt{u^2 + \varepsilon^2}}.$$

For  $h \in \mathbb{R}^d$ , define  $\psi_\varepsilon(h) \in \mathbb{R}^d$  entrywise:  $(\psi_\varepsilon(h))_j := \psi_\varepsilon(h_j)$ .

**Dataset-averaged smoothed  $\ell_1$  statistic.** Define

$$N_\varepsilon(t) := \frac{1}{n} \sum_{i=1}^n \frac{1}{d} \sum_{j=1}^d \rho_\varepsilon(h_{i,j}(t)). \quad (4.4)$$

Note that  $N_\varepsilon(t) \rightarrow \frac{1}{n} \sum_{i=1}^n S_{L_1}(h_i(t))$  as  $\varepsilon \rightarrow 0$ .

#### 4.4.4 Drift identity for $N_\varepsilon$

Define the drift components

$$\begin{aligned} D_\varepsilon(t) &:= \frac{1}{n^2 d} \sum_{i=1}^n \sum_{k=1}^n K_{ik}(t) \langle \psi_\varepsilon(h_i(t)), g_k(t) \rangle, \\ C_\varepsilon(t) &:= \frac{\lambda_h}{nd} \sum_{i=1}^n \sum_{j=1}^d \frac{h_{i,j}(t)^2}{\sqrt{h_{i,j}(t)^2 + \varepsilon^2}}, \\ R_\varepsilon(t) &:= \frac{1}{nd} \sum_{i=1}^n \langle \psi_\varepsilon(h_i(t)), r_i(t) \rangle. \end{aligned} \quad (4.5)$$

**Lemma 4.2** (Exact drift identity). For all  $t$  for which the trajectories are differentiable,

$$\dot{N}_\varepsilon(t) = -D_\varepsilon(t) - C_\varepsilon(t) + R_\varepsilon(t).$$

*Proof.* Differentiate (4.4):

$$\begin{aligned} \dot{N}_\varepsilon(t) &= \frac{1}{nd} \sum_{i=1}^n \sum_{j=1}^d \psi_\varepsilon(h_{i,j}(t)) \dot{h}_{i,j}(t) \\ &= \frac{1}{nd} \sum_{i=1}^n \langle \psi_\varepsilon(h_i(t)), \dot{h}_i(t) \rangle. \end{aligned}$$

Substitute (4.3) and identify terms using (4.5). □

**Lemma 4.3** (Two-sided decay bound). For all  $t$ ,

$$\lambda_h(N_\varepsilon(t) - \varepsilon) \leq C_\varepsilon(t) \leq \lambda_h N_\varepsilon(t).$$

Consequently,

$$\begin{aligned} -D_\varepsilon(t) - \lambda_h N_\varepsilon(t) + R_\varepsilon(t) &\leq \dot{N}_\varepsilon(t) \\ &\leq -D_\varepsilon(t) - \lambda_h(N_\varepsilon(t) - \varepsilon) + R_\varepsilon(t). \end{aligned} \quad (4.6)$$

*Proof.* For any  $u \in \mathbb{R}$ ,

$$0 \leq \frac{u^2}{\sqrt{u^2 + \varepsilon^2}} \leq \sqrt{u^2 + \varepsilon^2} = \rho_\varepsilon(u),$$

$$\frac{u^2}{\sqrt{u^2 + \varepsilon^2}} = \rho_\varepsilon(u) - \frac{\varepsilon^2}{\rho_\varepsilon(u)} \geq \rho_\varepsilon(u) - \varepsilon,$$

since  $\rho_\varepsilon(u) \geq \varepsilon$ . Summing over  $(i, j)$  and multiplying by  $\lambda_h/(nd)$  yields the result, and then (4.6) follows from theorem 4.2.  $\square$

#### 4.4.5 Phase I: sparsification (early-time decrease trend + hitting a low level)

**Assumption 4.4** (Phase I boundedness on a budget horizon). Fix  $T_1 > 0$ . Assume that on  $t \in [0, T_1]$ :

- (i) Kernel bound:  $\kappa(t) := \max_{i,k} |K_{ik}(t)| \leq \kappa_0$ .
- (ii) Head bound:  $\|W(t)\|_{2 \rightarrow 2} \leq M_0$ .
- (iii) Residual bound:  $|R_\varepsilon(t)| \leq r_0$ .

**Lemma 4.5** (Uniform bound on  $|D_\varepsilon|$  on Phase I). Under theorem 4.4, for all  $t \in [0, T_1]$ , we have  $|D_\varepsilon(t)| \leq \kappa_0 \sqrt{2} M_0 / \sqrt{d}$ .

*Proof.* By definition,

$$|D_\varepsilon(t)| \leq \frac{1}{n^2 d} \sum_{i,k} |K_{ik}(t)| \cdot |\langle \psi_\varepsilon(h_i(t)), g_k(t) \rangle|.$$

Since  $|\psi_\varepsilon(u)| \leq 1$ ,  $\|\psi_\varepsilon(h_i)\|_2 \leq \sqrt{d}$ , hence  $|\langle \psi_\varepsilon(h_i), g_k \rangle| \leq \sqrt{d} \|g_k\|_2$ . Using (4.2),  $\|g_k\|_2 \leq \sqrt{2} \|W\|_{2 \rightarrow 2} \leq \sqrt{2} M_0$ , and  $|K_{ik}(t)| \leq \kappa_0$ . Summing over  $i, k$  yields

$$|D_\varepsilon(t)| \leq \frac{1}{n^2 d} \cdot (n^2) \cdot \kappa_0 \cdot (\sqrt{d}) \cdot (\sqrt{2} M_0) = \kappa_0 \frac{\sqrt{2} M_0}{\sqrt{d}}.$$

$\square$

**Lemma 4.6** (Phase I dynamic). Under theorem 4.4, define  $B_0 := \kappa_0 \sqrt{2} M_0 / \sqrt{d} + r_0$ . Then for all  $t \in [0, T_1]$ , we have

$$\dot{N}_\varepsilon(t) \leq -\lambda_h (N_\varepsilon(t) - \varepsilon) + B_0, \quad (4.7)$$

and therefore

$$N_\varepsilon(t) - \varepsilon \leq (N_\varepsilon(0) - \varepsilon) e^{-\lambda_h t} + \frac{B_0}{\lambda_h} (1 - e^{-\lambda_h t}). \quad (4.8)$$

*Proof.* From the upper comparison inequality (4.6),

$$\dot{N}_\varepsilon(t) \leq -D_\varepsilon(t) - \lambda_h (N_\varepsilon(t) - \varepsilon) + R_\varepsilon(t).$$

Use  $-D_\varepsilon(t) \leq |D_\varepsilon(t)|$ , theorem 4.5, and  $|R_\varepsilon(t)| \leq r_0$  to obtain (4.7). Solving the scalar comparison ODE yields (4.8) and the hitting-time claim.  $\square$

**Corollary 4.7** (Phase I decrease trend + certified hitting time). From Lemma 4.6, we directly have that  $\dot{N}_\varepsilon(t) < 0$  whenever  $N_\varepsilon(t) > \varepsilon + \frac{B_0}{\lambda_h}$ . Moreover, for any target level  $L > \varepsilon + \frac{B_0}{\lambda_h}$ , define the (comparison) hitting time

$$t_L := \frac{1}{\lambda_h} \log \left( \frac{N_\varepsilon(0) - \varepsilon - \frac{B_0}{\lambda_h}}{L - \varepsilon - \frac{B_0}{\lambda_h}} \right),$$

(where the logarithm is well-defined when  $N_\varepsilon(0) > \varepsilon + \frac{B_0}{\lambda_h}$ ). If  $t_L \leq T_1$ , then  $N_\varepsilon(t_L) \leq L$ .

**Remark 4.8** (What Phase I does and does not claim). Phase I certifies (i) an early-time decrease trend whenever  $N_\varepsilon$  is above  $\varepsilon + \frac{B_0}{\lambda_h}$ , and (ii) the existence of a time  $t_L \leq T_1$  at which  $N_\varepsilon(t_L)$  reaches any prescribed level  $L > \varepsilon + \frac{B_0}{\lambda_h}$ . It does not claim monotone decrease beyond the certified horizon.

#### 4.4.6 Phase II: densification on a prescribed finite horizon

**Assumption 4.9** (Phase II one-shot densification assumption). There is a start time  $\tau > 0$  and horizon length  $H > 0$  that make the following conditions hold for every  $t \in [\tau, \tau + H]$ .

**(A) Boundedness and residual controls.** There exist constants  $\kappa_0, M, r_0, r_h \geq 0$  such that  $\kappa(t) := \max_{i,k \in [n]} |K_{ik}(t)| \leq \kappa_0$ ,  $\|W(t)\|_{2 \rightarrow 2} \leq M$ ,  $|R_\varepsilon(t)| \leq r_0$ ,  $\max_{i \in [n]} \|r_i(t)\|_2 \leq r_h$ .

**(B) Hard aligned subset with weak cross-talk.** There exist a subset  $S \subset [n]$  with  $|S| \geq \rho n$  and constants  $k_{\min} > 0$ ,  $\delta \in [0, 1)$ ,  $\alpha_0 > 0$ ,  $m_0 > 0$ ,  $a_0 > 0$  such that for all  $i \in S$  and all  $t \in [\tau, \tau + H]$ , we have  $K_{ii}(t) \geq k_{\min}$ ,  $\sum_{k \neq i} |K_{ik}(t)| \leq \delta K_{ii}(t)$ , and  $\alpha_i(t) := 1 - (p_i(t))_{y_i} \geq \alpha_0$ . Letting  $c_i(t) \in \arg \max_{c \neq y_i} z_{i,c}(t)$  (a highest-scoring wrong class), we have

$$z_{i,c_i(t)}(t) - \max_{c \neq y_i, c \neq c_i(t)} z_{i,c}(t) \geq m_0,$$

and with  $v_i(t) := W_{y_i}(t) - W_{c_i(t)}(t)$ ,

$$\langle \psi_\varepsilon(h_i(t)), v_i(t) \rangle \geq a_0 \sqrt{d}.$$

**(C) Easy complement + weak coupling to hard gradients.** There exist constants  $\bar{\alpha} \in (0, 1)$  and  $\bar{\delta} \geq 0$  such that for all  $t \in [\tau, \tau + H]$ , we have

$$\alpha_k(t) := 1 - (p_k(t))_{y_k} \leq \bar{\alpha} \quad \forall k \notin S,$$

$$\sum_{k \in S} \sum_{i \notin S} |K_{ik}(t)| \leq \bar{\delta} |S| k_{\min}.$$

**(D) Feasibility (signal dominates leakage and residual).** Define  $\zeta := (C-2)e^{-m_0}$ ,  $b_0 := (\alpha_0 - \zeta)a_0 - 2\zeta M$ ,  $\mu_D := \rho k_{\min} (b_0 - \delta \sqrt{2} M) / n \sqrt{d}$ ,  $\gamma_{\text{easy}} := \kappa_0 \sqrt{2} M (\sqrt{\bar{\alpha}} + \bar{\delta}) / \sqrt{d}$  and  $\mu_D^{\text{eff}} := \mu_D - \gamma_{\text{easy}}$ . Assume  $b_0 > \delta \sqrt{2} M$  and  $\mu_D^{\text{eff}} > r_0$ .

**(E) Initial margin below the Phase II threshold for the full horizon.** Let  $N_* := (\mu_D^{\text{eff}} - r_0) / \lambda_h$ . Define  $D_{\max} := \kappa_0 \sqrt{2} M / \sqrt{d}$ ,  $H_0 := \max_{i \in [n]} \|h_i(\tau)\|_2$  and

$$H_{\max} := e^{\lambda_h H} H_0 + \frac{\kappa_0 \sqrt{2} M + r_h}{\lambda_h} (e^{\lambda_h H} - 1),$$

$$N_{\max} := \frac{H_{\max}}{\sqrt{d}} + \varepsilon, \quad V := D_{\max} + \lambda_h N_{\max} + r_0.$$

Assume there exists  $\eta > 0$  such that

$$N_\varepsilon(\tau) \leq N_* - VH - \eta. \quad (4.9)$$

**Lemma 4.10** (Top-2 dominance from runner-up separation). Assume theorem 4.9(B) holds. Then for any  $i \in S$  and any  $t \in [\tau, \tau + H]$ ,

$$\begin{aligned} \sum_{c \neq y_i, c \neq c_i(t)} (p_i(t))_c &\leq (C-2)e^{-m_0} =: \zeta, \\ (p_i(t))_{c_i(t)} &\geq \alpha_i(t) - \zeta. \end{aligned}$$

*Proof.* Fix  $i \in S$  and  $t \in [\tau, \tau + H]$ . For any  $c \neq y_i, c_i(t)$ ,

$$\frac{(p_i(t))_c}{(p_i(t))_{c_i(t)}} = \exp(z_{i,c}(t) - z_{i,c_i(t)}(t)) \leq e^{-m_0}.$$

Summing over  $c \neq y_i, c_i(t)$  yields

$$\begin{aligned} \sum_{c \neq y_i, c \neq c_i(t)} (p_i(t))_c &\leq (C-2)e^{-m_0} (p_i(t))_{c_i(t)} \\ &\leq (C-2)e^{-m_0} = \zeta. \end{aligned}$$

Since  $\alpha_i(t) = \sum_{c \neq y_i} (p_i(t))_c = (p_i(t))_{c_i(t)} + \sum_{c \neq y_i, c \neq c_i(t)} (p_i(t))_c$ , we obtain  $(p_i(t))_{c_i(t)} \geq \alpha_i(t) - \zeta$ .  $\square$

**Lemma 4.11** (Diagonal negativity on  $S$ ). Assume theorem 4.9(A)–(D) holds. Then for all  $i \in S$  and  $t \in [\tau, \tau + H]$ ,

$$\langle \psi_\varepsilon(h_i(t)), g_i(t) \rangle \leq -b_0 \sqrt{d}.$$

*Proof.* Fix  $i \in S$  and  $t \in [\tau, \tau + H]$ . Recall

$$\begin{aligned} g_i(t) &= W(t)^\top (p_i(t) - e_{y_i}) \\ &= - \sum_{c \neq y_i} (p_i(t))_c (W_{y_i}(t) - W_c(t)). \end{aligned}$$

Hence

$$\begin{aligned} \langle \psi_\varepsilon(h_i), g_i \rangle &= -(p_i)_{c_i} \langle \psi_\varepsilon(h_i), v_i \rangle \\ &\quad - \sum_{c \neq y_i, c \neq c_i} (p_i)_c \langle \psi_\varepsilon(h_i), W_{y_i} - W_c \rangle. \end{aligned}$$

By alignment,  $\langle \psi_\varepsilon(h_i), v_i \rangle \geq a_0 \sqrt{d}$ . Also  $\|\psi_\varepsilon(h_i)\|_2 \leq \sqrt{d}$  and  $\|W_{y_i} - W_c\|_2 \leq 2\|W\|_{2 \rightarrow 2} \leq 2M$ , so  $|\langle \psi_\varepsilon(h_i), W_{y_i} - W_c \rangle| \leq 2M\sqrt{d}$ . Using theorem 4.10 and  $\alpha_i(t) \geq \alpha_0$  gives  $(p_i)_{c_i} \geq \alpha_0 - \zeta$  and  $\sum_{c \neq y_i, c \neq c_i} (p_i)_c \leq \zeta$ . Therefore

$$\begin{aligned} \langle \psi_\varepsilon(h_i), g_i \rangle &\leq -(\alpha_0 - \zeta)a_0 \sqrt{d} + (2M\sqrt{d})\zeta \\ &= -((\alpha_0 - \zeta)a_0 - 2\zeta M)\sqrt{d} = -b_0 \sqrt{d}. \end{aligned}$$

$\square$

**Lemma 4.12** (Uniform negativity of  $D_\varepsilon$  on the Phase II window (with easy-complement control)). Assume Assumption 4.9(B)–(E) hold. Then for all  $t \in [\tau, \tau + H]$ , we have  $D_\varepsilon(t) \leq -\mu_D^{\text{eff}}$ .

*Proof.* Fix  $t \in [\tau, \tau + H]$ . Decompose

$$\begin{aligned} D_\varepsilon(t) &= \frac{1}{n^2 d} \sum_{i \in S} \sum_{k=1}^n K_{ik}(t) \langle \psi_\varepsilon(h_i(t)), g_k(t) \rangle \\ &\quad + \frac{1}{n^2 d} \sum_{i \notin S} \sum_{k=1}^n K_{ik}(t) \langle \psi_\varepsilon(h_i(t)), g_k(t) \rangle \\ &=: D_S(t) + D_{S^c}(t). \end{aligned}$$

**Step 1: bound  $D_S(t)$  by a negative constant.** As in the original proof, for  $i \in S$  we have (Lemma 4.11)  $\langle \psi_\varepsilon(h_i(t)), g_i(t) \rangle \leq -b_0 \sqrt{d}$ , and for all  $i, k$  we have  $|\langle \psi_\varepsilon(h_i(t)), g_k(t) \rangle| \leq \sqrt{2} M \sqrt{d}$  (using  $\|\psi_\varepsilon(h_i)\|_2 \leq \sqrt{d}$  and  $\|g_k\|_2 \leq \sqrt{2} M$ ). Combining with weak cross-talk  $\sum_{k \neq i} |K_{ik}| \leq \delta K_{ii}$  and  $K_{ii} \geq k_{\min}$ ,  $|S| \geq \rho n$ , we obtain  $D_S(t) \leq \rho k_{\min} (\delta \sqrt{2} M - b_0) / n \sqrt{d} = -\mu_D$ .

**Step 2: bound the complement term  $D_{S^c}(t)$  using (C).** Split  $D_{S^c}(t)$  by  $k \in S$  and  $k \notin S$ :

$$\begin{aligned} D_{S^c}(t) &= \frac{1}{n^2 d} \sum_{i \notin S} \sum_{k \in S} K_{ik} \langle \psi(h_i), g_k \rangle \\ &\quad + \frac{1}{n^2 d} \sum_{i \notin S} \sum_{k \notin S} K_{ik} \langle \psi(h_i), g_k \rangle \\ &=: T_{\text{hard}}(t) + T_{\text{easy}}(t). \end{aligned}$$

*Easy-gradient part.* For  $k \notin S$ , (C) gives  $\alpha_k(t) \leq \bar{\alpha}$ , hence

$$\begin{aligned} \|g_k(t)\|_2 &\leq \|W(t)\|_{2 \rightarrow 2} \|p_k(t) - e_{y_k}\|_2 \\ &\leq M \sqrt{2 \alpha_k(t)} \\ &\leq \sqrt{2} M \sqrt{\bar{\alpha}}. \end{aligned}$$

Therefore  $|\langle \psi(h_i), g_k \rangle| \leq \|\psi(h_i)\|_2 \|g_k\|_2 \leq \sqrt{d} \cdot \sqrt{2} M \sqrt{\bar{\alpha}}$ , so with  $|K_{ik}| \leq \kappa_0$ ,

$$\begin{aligned} |T_{\text{easy}}(t)| &\leq \frac{1}{n^2 d} \sum_{i \notin S} \sum_{k \notin S} |K_{ik}| \cdot \sqrt{d} (\sqrt{2} M \sqrt{\bar{\alpha}}) \\ &\leq \frac{1}{n^2 d} \cdot n^2 \cdot \kappa_0 \cdot \sqrt{d} (\sqrt{2} M \sqrt{\bar{\alpha}}) = \frac{\kappa_0 \sqrt{2} M}{\sqrt{d}} \sqrt{\bar{\alpha}}. \end{aligned}$$

*Hard-gradient coupling from  $i \notin S$  to  $k \in S$ .* For  $k \in S$ , we use the crude bound  $\|g_k(t)\|_2 \leq \sqrt{2} M$ , hence  $|\langle \psi(h_i), g_k \rangle| \leq \sqrt{d} \cdot \sqrt{2} M$ . Thus

$$\begin{aligned} |T_{\text{hard}}(t)| &\leq \frac{1}{n^2 d} \sum_{i \notin S} \sum_{k \in S} |K_{ik}| \cdot \sqrt{d} (\sqrt{2} M) \\ &= \frac{\sqrt{2} M}{n^2 \sqrt{d}} \sum_{k \in S} \sum_{i \notin S} |K_{ik}|. \end{aligned}$$

By (C),  $\sum_{k \in S} \sum_{i \notin S} |K_{ik}| \leq \bar{\delta} |S| k_{\min} \leq \bar{\delta} (\rho n) k_{\min}$ , so

$$\begin{aligned} |T_{\text{hard}}(t)| &\leq \frac{\sqrt{2} M}{n^2 \sqrt{d}} \cdot \bar{\delta} (\rho n) k_{\min} = \frac{\rho k_{\min}}{n \sqrt{d}} \bar{\delta} \sqrt{2} M \\ &\leq \frac{\kappa_0 \sqrt{2} M}{\sqrt{d}} \bar{\delta}, \end{aligned}$$

where in the last step we used  $\rho k_{\min}/n \leq \kappa_0$  (since  $k_{\min} \leq \max_{i,k} |K_{ik}| \leq \kappa_0$  and  $\rho \leq 1$ ). Therefore

$$\begin{aligned} |D_{S^c}(t)| &\leq |T_{\text{hard}}(t)| + |T_{\text{easy}}(t)| \\ &\leq \frac{\kappa_0 \sqrt{2} M}{\sqrt{d}} (\bar{\delta} + \sqrt{\bar{\alpha}}) = \gamma_{\text{easy}}. \end{aligned}$$

**Step 3: combine.** We have  $D_\varepsilon(t) = D_S(t) + D_{S^c}(t) \leq -\mu_D + |D_{S^c}(t)| \leq -\mu_D + \gamma_{\text{easy}} = -\mu_D^{\text{eff}}$ .  $\square$

**Lemma 4.13** (Finite-velocity bound). Assume theorem 4.9(A) holds. With  $V$  as in theorem 4.9(E),

$$|\dot{N}_\varepsilon(t)| \leq V \quad \forall t \in [\tau, \tau + H].$$

*Proof.* From theorem 4.2,

$$|\dot{N}_\varepsilon| \leq |D_\varepsilon| + |C_\varepsilon| + |R_\varepsilon|.$$

Under (A), applying theorem 4.5 with  $(\kappa_0, M)$  gives  $|D_\varepsilon(t)| \leq D_{\max}$ . Also theorem 4.3 implies  $0 \leq C_\varepsilon(t) \leq \lambda_h N_\varepsilon(t)$ . It remains to bound  $N_\varepsilon(t)$  on  $[\tau, \tau + H]$ . From (4.3), we have

$$\begin{aligned} &\|\dot{h}_i(t)\|_2 \\ &\leq \frac{1}{n} \sum_k |K_{ik}(t)| \|g_k(t)\|_2 + \lambda_h \|h_i(t)\|_2 + \|r_i(t)\|_2 \\ &\leq \kappa_0 \sqrt{2} M + \lambda_h \|h_i(t)\|_2 + r_h, \end{aligned}$$

where we used  $\frac{1}{n} \sum_k |K_{ik}| \leq \max_k |K_{ik}| \leq \kappa_0$  and (4.2). Let  $u_i(t) := \|h_i(t)\|_2$ . Then  $u_i'(t) \leq \kappa_0 \sqrt{2} M + \lambda_h u_i(t) + r_h$ , so comparison yields  $u_i(t) \leq H_{\max}$  for all  $t \in [\tau, \tau + H]$ . Using  $\rho_\varepsilon(u) \leq |u| + \varepsilon$  and  $\|h_i\|_1 \leq \sqrt{d} \|h_i\|_2$  gives  $N_\varepsilon(t) \leq N_{\max}$ , hence  $|C_\varepsilon(t)| \leq \lambda_h N_{\max}$ . Finally, (A) gives  $|R_\varepsilon(t)| \leq r_0$ . Combining:  $|\dot{N}_\varepsilon(t)| \leq D_{\max} + \lambda_h N_{\max} + r_0 = V$ .  $\square$

**Theorem 4.14** (Phase II densification on a prescribed horizon). Under theorem 4.9,  $N_\varepsilon(t)$  is strictly increasing on  $[\tau, \tau + H]$  and

$$\dot{N}_\varepsilon(t) \geq \lambda_h \eta \quad \forall t \in [\tau, \tau + H].$$

*Proof.* By theorem 4.12,  $D_\varepsilon(t) \leq -\mu_D^{\text{eff}}$  for all  $t \in [\tau, \tau + H]$ . Also theorem 4.3 gives  $C_\varepsilon(t) \leq \lambda_h N_\varepsilon(t)$ , and (B) gives  $R_\varepsilon(t) \geq -r_0$ . Thus, for all  $t \in [\tau, \tau + H]$ ,

$$\begin{aligned} \dot{N}_\varepsilon(t) &= -D_\varepsilon(t) - C_\varepsilon(t) + R_\varepsilon(t) \\ &\geq \mu_D^{\text{eff}} - \lambda_h N_\varepsilon(t) - r_0 = \lambda_h (N_* - N_\varepsilon(t)). \end{aligned}$$

By theorem 4.13,  $|\dot{N}_\varepsilon(t)| \leq V$ , hence for any  $t \in [\tau, \tau + H]$ ,

$$N_\varepsilon(t) \leq N_\varepsilon(\tau) + V(t - \tau) \leq N_\varepsilon(\tau) + VH \leq N_* - \eta$$

using (4.9). Therefore  $N_* - N_\varepsilon(t) \geq \eta$  and so

$$\dot{N}_\varepsilon(t) \geq \lambda_h \eta \quad \forall t \in [\tau, \tau + H].$$

This implies strict increase on the whole window.  $\square$

#### 4.4.7 Finite-horizon U-shape: Phase I decrease trend + bridge to Phase II

**Theorem 4.15** (Finite-horizon sparsify-then-densify trigger). Assume Phase I boundedness (theorem 4.4) holds on  $[0, T_1]$  and that  $\lambda_h > 0$ . Let  $B_0$  be as in theorem 4.6.

**(1) Phase I: early decrease and certified entry into a low- $\ell_1$  regime.** For any level  $L > \varepsilon + \frac{B_0}{\lambda_h}$ , define  $t_L$  as in theorem 4.6. If  $t_L \leq T_1$ , then:

- (i)  $N_\varepsilon(t)$  is strictly decreasing whenever  $N_\varepsilon(t) > \varepsilon + \frac{B_0}{\lambda_h}$ ;
- (ii)  $N_\varepsilon(t_L) \leq L$  (so the trajectory reaches the prescribed low level by time  $t_L$ ).

**(2) Phase II trigger: densification on any later valid window.** Fix any horizon length  $H > 0$ . Suppose that at some (a priori unknown) later time  $\tau \geq 0$ , the Phase II assumptions (theorem 4.9) hold on the window  $[\tau, \tau + H]$ . Then on that window,  $N_\varepsilon$  is strictly increasing with the uniform slope lower bound

$$\dot{N}_\varepsilon(t) \geq \lambda_h \eta, \quad \forall t \in [\tau, \tau + H],$$

where  $\eta$  is the margin parameter appearing in theorem 4.9.

*Proof.* Part (1) is exactly theorem 4.6. Part (2) is exactly theorem 4.14 applied to the (hypothetical) window  $[\tau, \tau + H]$ .  $\square$

**Remark 4.16** (How to read the certificate). This theorem does *not* claim that a single continuous interval exhibits a full U-shape without further information. Instead it provides two independent, checkable guarantees along a training trajectory: (i) an *early-time sparsification certificate* that forces  $N_\varepsilon$  to decrease and reach any prescribed reasonable level  $L > \varepsilon + \frac{B_0}{\lambda_h}$  within the Phase I validity horizon, and (ii) a *densification trigger*: whenever (at any later time) the trajectory enters a finite window on which the persistent-hardness and alignment conditions of theorem 4.9 hold,  $N_\varepsilon$  must increase throughout that window at rate at least  $\lambda_h \eta$ . In this sense, a U-shape pattern arises whenever the dynamics first satisfy the Phase I conditions and later *activates* a Phase II window.

## 5 RQ3: How can this sparsity signal be practically leveraged to enhance model reasoning capabilities?

Based on our insight that the last hidden representation sparsity serves as a reliable rule for task complexity, we propose a novel few-shot example selection strategy for LLM reasoning: ***Sparsity-Guided Curriculum In-Context Learning (SG-ICL)***. While standard in-context learning often selects demonstrations randomly or relies solely on semantic similarity, such as (Ma et al., 2023) or Auto-CoT (Zhang et al., 2023), it ignores the cognitive load required to process them. We argue that an effective prompt should act as a *developmental curriculum*, guiding the model from rote, simple pattern matching to complex reasoning.

First, we assess the difficulty of all candidate examples in the demonstration pool. We compute the sparsity score  $S(x)$  for each example  $x$  using the  $L_1$  norm of its last hidden state  $\mathbf{h}_L$ . We then sort the examples and group them into  $K$  distinct difficulty levels (or bins)  $\mathcal{B}_1, \dots, \mathcal{B}_K$ :

$$S(x) = \|\mathbf{h}_L(x)\|_1, \text{ with } x \in \mathcal{B}_k \Leftrightarrow \tau_{k-1} \leq S(x) < \tau_k \quad (5.1)$$

Here,  $\tau$  represents the threshold boundaries derived from the percentiles of the sparsity distribution, allowing us to categorize examples from “Easy” to “Hard” systematically. During the inference phase for a specific test query  $x_{query}$ , our strategy employs a ***dual-criteria*** selection process:

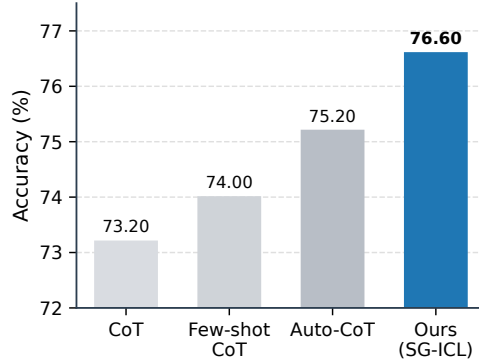


Figure 7: **Performance Comparison of Reasoning Strategies.** Our proposed Sparsity-Guided Curriculum In-Context Learning (SG-ICL) achieves an accuracy of 76.60% on MATH-500 with Qwen2.5-7B, substantially outperforming standard CoT baselines (zero-shot and few-shot) as well as the strong Auto-CoT baseline (75.20%).

1. **Semantic Filtering:** We first retrieve a candidate set  $\mathcal{N}_{sem}$  consisting of the top- $N$  examples most semantically similar to  $x_{query}$  by leveraging Sentence-BERT (Reimers and Gurevych, 2019) to compute dense vector embeddings.
2. **Difficulty Matching:** We then calculate the sparsity  $S(x_{query})$  of the incoming query  $x_{query}$  to identify its corresponding difficulty level  $\mathcal{B}_{target}$ . From  $\mathcal{N}_{sem}$ , we specifically select  $k$  examples that not only maintain high semantic similarity but also align with the target difficulty level (i.e., falling within  $\mathcal{B}_{target}$ ).

This process ensures the few-shot prompt is both contextually relevant and cognitively aligned with the query’s content and complexity.

To validate this approach, we conducted extensive experiments on the Qwen2.5-7B model. Empirical results on the MATH-500 dataset demonstrate that our Sparsity-Guided Curriculum strategy significantly outperforms strong baselines, including Auto-CoT and random selection, proving that incorporating Curriculum into the retrieval process yields substantial gains in reasoning accuracy, as illustrated in Figure 7. Furthermore, we extended the application of our sparsity metric beyond inference-time retrieval to the training phase, organizing training data from easy to hard.

## 6 Conclusion

In this work, we have established a fundamental connection between the internal representation geometry of Large Language Models and the difficulty of the tasks they face. Through a rigorous analysis across diverse models, benchmarks, and OOD settings, we validated the phenomenon that *“the farther the shift, the sparser the representation.”* Our findings reveal that this sparsification is not a random artifact but a consistent, adaptive mechanism localized primarily in the final transformer layers, acting as a selective filter to stabilize reasoning under uncertainty. Ultimately, our study bridges the gap between mechanistic interpretability and the reasoning domain, offering a new perspective on how LLMs internalize complexity. We hope this work inspires future research like sparsity-aware training objectives.

## 7 Acknowledgement

I am grateful to Fei Sun, Jinman Zhao, Mengru Wang, and Zirui Liu for many helpful discussions that improved this paper. And I would like to especially thank Zirui Liu, Minghao Guo, and Xi Zhu for their encouragement and support throughout the process.

## References

- Armen Aghajanyan, Sonal Gupta, and Luke Zettlemoyer. 2021. Intrinsic Dimensionality Explains the Effectiveness of Language Model Fine-Tuning. In *Proceedings of the 59th Annual Meeting of the Association for Computational Linguistics and the 11th International Joint Conference on Natural Language Processing (ACL-IJCNLP)*, pages 7319–7328.
- Iván Arcuschin, Jett Janiak, Robert Krzyzanowski, Senthooan Rajamanoharan, Neel Nanda, and Arthur Conmy. 2025. **Chain-of-thought reasoning in the wild is not always faithful**. In *Workshop on Reasoning and Planning for Large Language Models*.
- Nora Belrose, Zach Furman, Logan Smith, Danny Halawi, Igor Ostrovsky, Lev McKinney, Stella Biderman, and Jacob Steinhardt. 2023. Eliciting latent predictions from transformers with the tuned lens. *arXiv preprint arXiv:2303.08112*.
- Yoshua Bengio, Jérôme Louradour, Ronan Collobert, and Jason Weston. 2009. **Curriculum learning**. In *International Conference on Machine Learning (ICML)*.
- Trenton Bricken, Adly Templeton, Joshua Batson, Brian Chen, Adam Jermyn, Tom Conerly, Nick Turner, Cem Kundu, Shan Carter, Tom Henighan, and 1 others. 2023. **Towards monosemanticity: Decomposing language models with dictionary learning**. *Transformer Circuits Thread (Anthropic Technique report)*.
- Shiqi Chen, Yiran Zhao, Jinghan Zhang, I-Chun Chern, Siyang Gao, Pengfei Liu, and Junxian He. 2023. **FELM: Benchmarking factuality evaluation of large language models**. In *Thirty-seventh Conference on Neural Information Processing Systems Datasets and Benchmarks Track (NeurIPS)*.
- Tianlong Chen, Jonathan Frankle, Shiyu Chang, Sijia Liu, Yang Zhang, Zhangyang Wang, and Michael Carbin. 2020. The lottery ticket hypothesis for pre-trained bert networks. In *Advances in Neural Information Processing Systems (NeurIPS)*.
- Hongrong Cheng, Miao Zhang, and Javen Qinfeng Shi. 2024. A survey on deep neural network pruning: Taxonomy, comparison, analysis, and recommendations. *IEEE Transactions on Pattern Analysis and Machine Intelligence (TPAMI)*.
- Arthur Conmy, Augustine N Mavor-Parker, Aengus Lynch, Stefan Heimersheim, and Adrià Garriga-Alonso. 2023. Towards automated circuit discovery for mechanistic interpretability. In *Proceedings of the 37th International Conference on Neural Information Processing Systems (NeurIPS)*, pages 16318–16352.
- Nicola De Cao, Leon Schmid, Dieuwke Hupkes, and Ivan Titov. 2022. Sparse Interventions in Language Models with Differentiable Masking. In *Proceedings of the Fifth BlackboxNLP Workshop on Analyzing and Interpreting Neural Networks for NLP*, pages 16–27.

- Branton DeMoss, Silvia Sapora, Jakob Foerster, Nick Hawes, and Ingmar Posner. 2025. The complexity dynamics of grokking. *Physica D: Nonlinear Phenomena*, page 134859.
- Nelson Elhage, Tristan Hume, Catherine Olsson, Nicholas Schiefer, Tom Henighan, Shauna Kravec, Zac Hatfield-Dodds, Robert Lasenby, Dawn Drain, Carol Chen, Roger Grosse, Sam McCandlish, Jared Kaplan, Dario Amodei, Martin Wattenberg, and Christopher Olah. 2022. **Toy models of superposition**. *Transformer Circuits Thread (Anthropic Technique report)*.
- Nelson Elhage, Neel Nanda, Catherine Olsson, and 1 others. 2021. **A mathematical framework for transformer circuits**. *Transformer Circuits Thread (Anthropic Technique report)*.
- Jonathan Frankle and Michael Carbin. 2019. **The lottery ticket hypothesis: Finding sparse, trainable neural networks**. In *International Conference on Learning Representations (ICLR)*.
- Sandeep Reddy Gantla. 2025. Exploring mechanistic interpretability in large language models: Challenges, approaches, and insights. In *2025 International Conference on Data Science, Agents & Artificial Intelligence (ICDSAAI)*, pages 1–8. IEEE.
- Mor Geva, Roei Schuster, Jonathan Berant, and Omer Levy. 2021. Transformer feed-forward layers are key-value memories. In *Proceedings of the 2021 Conference on Empirical Methods in Natural Language Processing (EMNLP)*, pages 5484–5495.
- Asma Ghandeharioun, Avi Caciularu, Adam Pearce, Lucas Dixon, and Mor Geva. 2024. Patchscopes: A unifying framework for inspecting hidden representations of language models. In *International Conference on Machine Learning (ICML)*, pages 15466–15490. PMLR.
- Xavier Glorot, Antoine Bordes, and Yoshua Bengio. 2011. Deep sparse rectifier neural networks. In *International Conference on Artificial Intelligence and Statistics (AISTATS)*, pages 315–323. JMLR Workshop and Conference Proceedings.
- Mitchell Gordon, Kevin Duh, and Nicholas Andrews. 2020. Compressing bert: Studying the effects of weight pruning on transfer learning. In *Proceedings of the 5th Workshop on Representation Learning for NLP (ACL Workshop)*, pages 143–155.
- Jiaojiao Han, Wujiang Xu, Mingyu Jin, and Mengnan Du. 2025. Sage: An agentic explainer framework for interpreting sae features in language models. *arXiv preprint arXiv:2511.20820*.
- Song Han, Jeff Pool, John Tran, and William J Dally. 2015. Learning both weights and connections for efficient neural networks. In *Proceedings of the 29th International Conference on Neural Information Processing Systems (NeurIPS)*, pages 1135–1143.
- Zirui He, Mingyu Jin, Bo Shen, Ali Payani, Yongfeng Zhang, and Mengnan Du. 2025. Sae-ssv: Supervised steering in sparse representation spaces for reliable control of language models. *arXiv preprint arXiv:2505.16188*.
- Benjamin Heinzerling and Kentaro Inui. 2024. Monotonic Representation of Numeric Attributes in Language Models. In *Proceedings of the 62nd Annual Meeting of the Association for Computational Linguistics (ACL)*, pages 175–195.

- Dan Hendrycks, Collin Burns, Steven Basart, Andy Zou, Mantas Mazeika, Dawn Song, and Jacob Steinhardt. 2021. **Measuring massive multitask language understanding**. In *International Conference on Learning Representations (ICLR)*.
- John Hewitt and Christopher D. Manning. 2019. A Structural Probe for Finding Syntax in Word Representations. In *Proceedings of the 2019 Conference of the North American Chapter of the Association for Computational Linguistics: Human Language Technologies (NAACL)*, pages 4129–4138.
- Torsten Hoeffler, Dan Alistarh, Tal Ben-Nun, Nikoli Dryden, and Alexandra Peste. 2021. Sparsity in deep learning: Pruning and growth for efficient inference and training in neural networks. *Journal of Machine Learning Research (JMLR)*, 22(241):1–124.
- Edward J. Hu, Yelong Shen, Phillip Wallis, Zeyuan Allen-Zhu, Yuanzhi Li, Shean Wang, Lu Wang, and Weizhu Chen. 2022. LoRA: Low-Rank Adaptation of Large Language Models. In *International Conference on Learning Representations (ICLR)*.
- Robert Huben, Hoagy Cunningham, Logan Riggs Smith, Aidan Ewart, and Lee Sharkey. 2024. **Sparse autoencoders find highly interpretable features in language models**. In *The Twelfth International Conference on Learning Representations (ICLR)*.
- Ziwei Ji and Matus Telgarsky. 2019. **The implicit bias of gradient descent on nonseparable data**. In *Annual Conference Computational Learning Theory (COLT)*.
- Mingyu Jin, Weidi Luo, Sitao Cheng, Xinyi Wang, Wenyue Hua, Ruixiang Tang, William Yang Wang, and Yongfeng Zhang. 2025a. Disentangling memory and reasoning ability in large language models. In *Proceedings of the 63rd Annual Meeting of the Association for Computational Linguistics (Volume 1: Long Papers)*, pages 1681–1701.
- Mingyu Jin, Kai Mei, Wujiang Xu, Mingjie Sun, Ruixiang Tang, Mengnan Du, Zirui Liu, and Yongfeng Zhang. 2025b. **Massive values in self-attention modules are the key to contextual knowledge understanding**. In *Forty-second International Conference on Machine Learning*.
- Mingyu Jin, Qinkai Yu, Jingyuan Huang, Qingcheng Zeng, Zhenting Wang, Wenyue Hua, Haiyan Zhao, Kai Mei, Yanda Meng, Kaize Ding, and 1 others. 2025c. Exploring concept depth: How large language models acquire knowledge and concept at different layers? In *Proceedings of the 31st international conference on computational linguistics*, pages 558–573.
- Pang Wei Koh, Shiori Sagawa, Henrik Marklund, Sang Michael Xie, Marvin Zhang, Akshay Balsubramani, Weihua Hu, Michihiro Yasunaga, Richard Lanus Phillips, Irena Gao, and 1 others. 2021. Wilds: A benchmark of in-the-wild distribution shifts. In *International conference on machine learning (ICML)*, pages 5637–5664. PMLR.
- Tanishq Kumar, Blake Bordelon, Samuel J. Gershman, and Cengiz Pehlevan. 2024. **Grokking as the transition from lazy to rich training dynamics**. In *The Twelfth International Conference on Learning Representations (ICLR)*.
- Tamera Lanham, Anna Chen, Ansh Radhakrishnan, Benoit Steiner, Carson Denison, Danny Hernandez, Dustin Li, Esin Durmus, Evan Hubinger, Jackson Kernion, and 1 others. 2023. Measuring faithfulness in chain-of-thought reasoning. *arXiv preprint arXiv:2307.13702*.

- Mingyu Lee, Jun Hyung Park, Junho Kim, Kang Min Kim, and Sang Keun Lee. 2022. Efficient pre-training of masked language model via concept-based curriculum masking. In *2022 Conference on Empirical Methods in Natural Language Processing (EMNLP)*, pages 7417–7427.
- Tianle Li, Ge Zhang, Quy Duc Do, Xiang Yue, and Wenhui Chen. 2025a. **Long-context LLMs struggle with long in-context learning**. *Transactions on Machine Learning Research (TMLR)*.
- Zhong-Zhi Li, Duzhen Zhang, Ming-Liang Zhang, Jiabin Zhang, Zengyan Liu, Yuxuan Yao, Haotian Xu, Junhao Zheng, Pei-Jie Wang, Xiuyi Chen, and 1 others. 2025b. From system 1 to system 2: A survey of reasoning large language models. *IEEE transactions on pattern analysis and machine intelligence (TPAMI)*.
- Zonglin Li, Chong You, Srinadh Bhojanapalli, Daliang Li, Ankit Singh Rawat, Sashank J. Reddi, Ke Ye, Felix Chern, Felix Yu, Ruiqi Guo, and Sanjiv Kumar. 2023. **The lazy neuron phenomenon: On emergence of activation sparsity in transformers**. In *The Eleventh International Conference on Learning Representations (ICLR)*.
- Hunter Lightman, Vineet Kosaraju, Yuri Burda, Harrison Edwards, Bowen Baker, Teddy Lee, Jan Leike, John Schulman, Ilya Sutskever, and Karl Cobbe. 2024. **Let’s verify step by step**. In *The Twelfth International Conference on Learning Representations (ICLR)*.
- James Liu, Pragaash Ponnusamy, Tianle Cai, Han Guo, Yoon Kim, and Ben Athiwaratkun. 2025. Training-free activation sparsity in large language models. In *International Conference on Learning Representations (ICLR)*.
- Zichang Liu, Jue Wang, Tri Dao, Tianyi Zhou, Binhang Yuan, Zhao Song, Anshumali Shrivastava, Ce Zhang, Yuandong Tian, Christopher Re, and 1 others. 2023. Deja vu: Contextual sparsity for efficient llms at inference time. In *International Conference on Machine Learning (ICML)*, pages 22137–22176. PMLR.
- Haipeng Luo, Qingfeng Sun, Can Xu, Pu Zhao, Jian-Guang Lou, Chongyang Tao, Xiubo Geng, Qingwei Lin, Shifeng Chen, Yansong Tang, and Dongmei Zhang. 2025. **Wizardmath: Empowering mathematical reasoning for large language models via reinforced evol-instruct**. In *The Thirteenth International Conference on Learning Representations (ICLR)*.
- Xinbei Ma, Yeyun Gong, Pengcheng He, Hai Zhao, and Nan Duan. 2023. Query rewriting in retrieval-augmented large language models. In *Proceedings of the 2023 Conference on Empirical Methods in Natural Language Processing (EMNLP)*, pages 5303–5315.
- Kevin Meng, David Bau, Alex J Andonian, and Yonatan Belinkov. 2022. Locating and editing factual associations in gpt. In *Advances in Neural Information Processing Systems (NeurIPS)*.
- Subhabrata Mukherjee, Arindam Mitra, Ganesh Jawahar, Sahaj Agarwal, Hamid Palangi, and Ahmed Awadallah. 2023. Orca: Progressive learning from complex explanation traces of gpt-4. *arXiv preprint arXiv:2306.02707*.
- Mor Shpigel Nacson, Nathan Srebro, and Daniel Soudry. 2019. Stochastic gradient descent on separable data: Exact convergence with a fixed learning rate. In *The 22nd International Conference on Artificial Intelligence and Statistics (AISTAT)*, pages 3051–3059. PMLR.

- Koichi Nagatsuka, Clifford Broni-Bediako, and Masayasu Atsumi. 2021. **Pre-training a BERT with curriculum learning by increasing block-size of input text**. In *Proceedings of the International Conference on Recent Advances in Natural Language Processing (RANLP)*, pages 989–996.
- Jingcheng Niu, Xingdi Yuan, Tong Wang, Hamid Reza Saghir, and Amir H. Abdi. 2025. **Llama see, llama do: A mechanistic perspective on contextual entrainment and distraction in llms**. In *Annual Meeting of the Association for Computational Linguistics (ACL)*.
- nostalgebraist. 2020. interpreting gpt: the logit lens. <https://www.lesswrong.com/posts/AcKRB8wDpdaN6v6ru/interpreting-gpt-the-logit-lens>. Accessed: 2024-05-20.
- Bruno A Olshausen and David J Field. 1996. Emergence of simple-cell receptive field properties by learning a sparse code for natural images. *Nature*, 381(6583):607–609.
- Catherine Olsson, Nelson Elhage, Neel Nanda, Nicholas Joseph, Nova DasSarma, Tom Henighan, Ben Mann, Amanda Askell, Yuntao Bai, Anna Chen, and 1 others. 2022. **In-context learning and induction heads**. *Transformer Circuits Thread*.
- Emmanouil Antonios Platanios, Otilia Stretcu, Graham Neubig, Barnabas Poczos, and Tom Mitchell. 2019. Competence-based curriculum learning for neural machine translation. In *Proceedings of the 2019 conference of the North American chapter of the association for computational linguistics: human language technologies (NAACL)*, pages 1162–1172.
- Sai Prasanna, Anna Rogers, and Anna Rumshisky. 2020. When bert plays the lottery, all tickets are winning. In *Proceedings of the 2020 Conference on Empirical Methods in Natural Language Processing (EMNLP)*, pages 3208–3229.
- Zhenting Qi, Hongyin Luo, Xuliang Huang, Zhuokai Zhao, Yibo Jiang, Xiangjun Fan, Himabindu Lakkaraju, and James R. Glass. 2025. **Quantifying generalization complexity for large language models**. In *The Thirteenth International Conference on Learning Representations (ICLR)*.
- Nils Reimers and Iryna Gurevych. 2019. Sentence-bert: Sentence embeddings using siamese bert-networks. In *Proceedings of the 2019 Conference on Empirical Methods in Natural Language Processing and the 9th International Joint Conference on Natural Language Processing (EMNLP-IJCNLP)*, pages 3982–3992.
- Yi Ren and Danica J. Sutherland. 2025. Learning dynamics of llm finetuning. In *International Conference on Learning Representations (ICLR)*.
- Daniel Soudry, Elad Hoffer, Mor Shpigel Nacson, Suriya Gunasekar, and Nathan Srebro. 2018. The implicit bias of gradient descent on separable data. *Journal of Machine Learning Research*, 19(70):1–57.
- Valentin I Spitkovsky, Hiyan Alshawi, and Dan Jurafsky. 2010. From baby steps to leapfrog: How “less is more” in unsupervised dependency parsing. In *The 2010 Annual Conference of the North American Chapter of the Association for Computational Linguistics (NAACL)*, pages 751–759.
- Student. 1908. **The Probable Error of a Mean**. *Biometrika*, 6(1):1–25.
- Tongyi DeepResearch Team, Baixuan Li, Bo Zhang, Dingchu Zhang, Fei Huang, Guangyu Li, Guoxin Chen, Hui Feng Yin, Jialong Wu, Jingren Zhou, and 1 others. 2025. Tongyi deepresearch technical report. *ArXiv Preprint (Tongyi Qwen technical report)*.

- Hugo Touvron, Thibaut Lavril, Gautier Izacard, Xavier Martinet, Marie-Anne Lachaux, Timothée Lacroix, Baptiste Rozière, Naman Goyal, Eric Hambro, Faisal Azhar, and 1 others. 2023. Llama: Open and efficient foundation language models. *arXiv preprint arXiv:2302.13971*.
- Miles Turpin, Julian Michael, Ethan Perez, and Samuel R Bowman. 2023. Language models don't always say what they think: Unfaithful explanations in chain-of-thought prompting. In *Advances in Neural Information Processing Systems (NeurIPS)*.
- Boshi Wang, Xiang Yue, Yu Su, and Huan Sun. 2024a. Grokking of implicit reasoning in transformers: a mechanistic journey to the edge of generalization. In *Proceedings of the 38th International Conference on Neural Information Processing Systems (NeurIPS)*, pages 95238–95265.
- Kevin Ro Wang, Alexandre Variengien, Arthur Conmy, Buck Shlegeris, and Jacob Steinhardt. 2022. Interpretability in the Wild: A Circuit for Indirect Object Identification in GPT-2 Small. In *The Eleventh International Conference on Learning Representations (ICLR)*.
- Mengru Wang, Yunzhi Yao, Ziwen Xu, Shuofei Qiao, Shumin Deng, Peng Wang, Xiang Chen, Jia-Chen Gu, Yong Jiang, Pengjun Xie, and 1 others. 2024b. Knowledge mechanisms in large language models: A survey and perspective. In *Findings of the Association for Computational Linguistics: (EMNLP Findings)*, pages 7097–7135.
- Xin Wang, Yudong Chen, and Wenwu Zhu. 2021. A survey on curriculum learning. *IEEE transactions on pattern analysis and machine intelligence (TPAMI)*, 44(9):4555–4576.
- Xinyi Wang, Antonis Antoniadis, Yanai Elazar, Alfonso Amayuelas, Alon Albalak, Kexun Zhang, and William Yang Wang. 2025a. **Generalization v.s. memorization: Tracing language models' capabilities back to pretraining data**. In *The Thirteenth International Conference on Learning Representations (ICLR)*.
- Xinyi Wang, Shawn Tan, Mingyu Jin, William Yang Wang, Rameswar Panda, and Yikang Shen. 2025b. **Do larger language models imply better generalization? a pretraining scaling law for implicit reasoning**. In *ICML 2025 Workshop on Methods and Opportunities at Small Scale*.
- Yubo Wang, Xueguang Ma, Ge Zhang, Yuansheng Ni, Abhranil Chandra, Shiguang Guo, Weiming Ren, Aaran Arulraj, Xuan He, Ziyang Jiang, and 1 others. 2024c. MMLU-Pro: a more robust and challenging multi-task language understanding benchmark. In *Proceedings of the 38th International Conference on Neural Information Processing Systems (NeurIPS)*, pages 95266–95290.
- Zhenting Wang, Guofeng Cui, Yu-Jhe Li, Kun Wan, and Wentian Zhao. 2025c. Dump: Automated distribution-level curriculum learning for rl-based llm post-training. *arXiv preprint arXiv:2504.09710*.
- Jason Wei, Xuezhi Wang, Dale Schuurmans, Maarten Bosma, Brian Ichter, Fei Xia, Ed H Chi, Quoc V Le, and Denny Zhou. 2022. Chain-of-thought prompting elicits reasoning in large language models. In *Proceedings of the 36th International Conference on Neural Information Processing Systems (NeurIPS)*, pages 24824–24837.
- Chris Wendler, Veniamin Veselovsky, Giovanni Monea, and Robert West. 2024. Do llamas work in english? on the latent language of multilingual transformers. In *Proceedings of the 62nd Annual Meeting of the Association for Computational Linguistics (ACL)*, pages 15366–15394.

- Jing Xiong, Jianghan Shen, Fanghua Ye, Chaofan Tao, Zhongwei Wan, Jianqiao Lu, Xun Wu, Chuanyang Zheng, Zhijiang Guo, Min Yang, Lingpeng Kong, and Ngai Wong. 2025. UNComp: Can matrix entropy uncover sparsity? — a compressor design from an uncertainty-aware perspective. In *Proceedings of the 2025 Conference on Empirical Methods in Natural Language Processing (EMNLP)*.
- Benfeng Xu, Licheng Zhang, Zhendong Mao, Quan Wang, Hongtao Xie, and Yongdong Zhang. 2020. **Curriculum learning for natural language understanding**. In *Proceedings of the 58th Annual Meeting of the Association for Computational Linguistics (ACL)*, pages 6095–6104.
- Can Xu, Qingfeng Sun, Kai Zheng, Xiubo Geng, Pu Zhao, Jiazhan Feng, Chongyang Tao, Qingwei Lin, and Daxin Jiang. 2024. **WizardLM: Empowering large pre-trained language models to follow complex instructions**. In *The Twelfth International Conference on Learning Representations (ICLR)*.
- An Yang, Baosong Yang, Beichen Zhang, Binyuan Hui, Bo Zheng, Bowen Yu, Chengyuan Li, Dayiheng Liu, Fei Huang, Haoran Wei, and 1 others. 2024. Qwen2. 5 technical report. *arXiv preprint arXiv:2412.15115*.
- Jiaran Ye, Zijun Yao, Zhidian Huang, Liangming Pan, Jinxin Liu, Yushi Bai, Amy Xin, Liu Weichuan, Xiaoyin Che, Lei Hou, and Juanzi Li. 2025. **How do transformers learn implicit reasoning?** In *The Thirty-ninth Annual Conference on Neural Information Processing Systems (NeurIPS)*.
- Yutong Yin and Zhaoran Wang. 2025. **Are transformers able to reason by connecting separated knowledge in training data?** In *The Thirteenth International Conference on Learning Representations (ICLR)*.
- Chong Zhang, Mingyu Jin, Dong Shu, Taowen Wang, Dongfang Liu, and Xiaobo Jin. 2024a. Target-driven attack for large language models. In *ECAI*.
- Chong Zhang, Mingyu Jin, Qinkai Yu, Chengzhi Liu, Haochen Xue, and Xiaobo Jin. 2024b. Goal-guided generative prompt injection attack on large language models. In *2024 IEEE International Conference on Data Mining (ICDM)*, pages 941–946. IEEE.
- Zhuosheng Zhang, Aston Zhang, Mu Li, and Alex Smola. 2023. **Automatic chain of thought prompting in large language models**. In *The Eleventh International Conference on Learning Representations (ICLR)*.
- Haiyan Zhao, Hanjie Chen, Fan Yang, Ninghao Liu, Huiqi Deng, Hengyi Cai, Shuaiqiang Wang, Dawei Yin, and Mengnan Du. 2024a. Explainability for large language models: A survey. *ACM Transactions on Intelligent Systems and Technology*, 15(2):1–38.
- Haiyan Zhao, Fan Yang, Bo Shen, Himabindu Lakkaraju, and Mengnan Du. 2024b. Towards uncovering how large language model works: An explainability perspective. *arXiv preprint arXiv:2402.10688*.
- Haiyan Zhao, Heng Zhao, Bo Shen, Ali Payani, Fan Yang, and Mengnan Du. 2025. Beyond Single Concept Vector: Modeling Concept Subspace in LLMs with Gaussian Distribution. In *The Thirteenth International Conference on Learning Representations (ICLR)*.
- Yize Zhao, Tina Behnia, Vala Vakilian, and Christos Thrampoulidis. 2024c. **Implicit geometry of next-token prediction: From language sparsity patterns to model representations**. In *First Conference on Language Modeling (COLM)*.
- Yize Zhao and Christos Thrampoulidis. 2025a. **Geometry of concepts in next-token prediction: Neural-collapse meets semantics**. In *The Second Conference on Parsimony and Learning (CPAL)*.

Yize Zhao and Christos Thrampoulidis. 2025b. [On the geometry of semantics in next-token prediction](#). In *The First Workshop on the Interplay of Model Behavior and Model Internals (COLM Workshop)*.

Zihao Zhou, Qiufeng Wang, Mingyu Jin, Jie Yao, Jianan Ye, Wei Liu, Wei Wang, Xiaowei Huang, and Kaizhu Huang. 2024. Mathattack: Attacking large language models towards math solving ability. In *Proceedings of the AAAI Conference on Artificial Intelligence*, volume 38, pages 19750–19758.

## A Appendix

*“What I cannot create, I do not understand.”*

— Richard P. Feynman<sup>1</sup>

### A.1 Related Work

#### A.1.1 Sparsity in Deep Neural Network

Sparsity in deep learning is traditionally studied through two distinct lenses: computational efficiency and representational disentanglement (Hoeffler et al., 2021; Cheng et al., 2024).

From an efficiency perspective, weight sparsity aims to reduce model size and inference cost. Pioneering work in network pruning demonstrated that significant portions of parameters can be removed without performance degradation (Han et al., 2015). This line of inquiry culminated in the *Lottery Ticket Hypothesis*, which posits that dense networks contain sparse, trainable subnetworks capable of matching the original model’s accuracy (Frankle and Carbin, 2019). This hypothesis was subsequently extended to Transformer architectures, particularly BERT. Research indicates that pre-trained BERT models contain matching subnetworks at extreme sparsity levels (e.g., 40%–90%) that perform comparably on downstream tasks (Chen et al., 2020; Prasanna et al., 2020; Gordon et al., 2020).

Beyond imposed sparsity, recent empirical studies reveal that LLMs exhibit a high degree of *intrinsic activation sparsity*. Despite being trained as dense networks, the activations within Transformer Feed-Forward Networks (FFNs) are highly sparse, with only a small fraction of neurons firing for any given input token. This behavior, often termed the “Lazy Neuron” phenomenon, becomes more pronounced as model scale increases (Li et al., 2023).

Further analysis characterizes this as *contextual sparsity*: specific inputs activate predictable, sparse sub-graphs of the network, suggesting that LLMs implicitly learn modular structures without explicit architectural constraints (Liu et al., 2023; Jin et al., 2025b). Further analysis characterizes this as *contextual sparsity*: specific inputs activate predictable, sparse sub-graphs of the network, suggesting that LLMs implicitly learn modular structures without explicit architectural constraints (Liu et al., 2023). (Zhao and Thrampoulidis, 2025b,a; Zhao et al., 2024c) view language modeling as a classification problem of “predicting the distribution of the next word for each context,” the sparsity pattern of the language data strongly determines the geometry of the trained representation. They found that Next Token Prediction (NTP) training implicitly favors a “sparse + low-rank” structure in the logit space.

---

<sup>1</sup>This quotation is commonly attributed to Richard P. Feynman and was reportedly written on his office blackboard at the time of his death in 1988; see Smithsonian Magazine, [Learn Physics From Nobel Prizewinner Richard Feynman for Free](#).

### A.1.2 LLM Curriculum Reasoning:

Curriculum Learning (CL), introduced by (Bengio et al., 2009), is a training strategy that exposes models to examples in an easy-to-hard progression, rather than in random order (Wang et al., 2021). Early NLP applications likewise leveraged CL principles. In unsupervised grammar induction, a dependency parser was trained on short, simple sentences first and incrementally included longer, more complex sentences, yielding improved parsing accuracy (Spitkovsky et al., 2010). With the advent of deep learning, Curriculum Learning (CL) was widely adopted in Neural Machine Translation (NMT), where examples were typically sorted by sentence length or word rarity to accelerate convergence (Platanios et al., 2019; Xu et al., 2020). In the era of Pre-trained Language Models (PLMs) such as BERT, CL strategies shifted towards optimizing data scheduling to improve sample efficiency during the massive pre-training phase (Nagatsuka et al., 2021; Lee et al., 2022).

Most recently, the rise of LLMs has reinvigorated CL, particularly in enhancing complex reasoning capabilities and instruction following Wang et al. (2025c). Unlike traditional methods relying on superficial metrics (e.g., length), modern CL for LLMs focuses on *semantic complexity* and *reasoning depth*. For instance, Xu et al. (2024) proposed *Evol-Instruct*, a method that incrementally rewrites instructions to increase difficulty, effectively creating a curriculum for instruction tuning. Similarly, Mukherjee et al. (2023) demonstrated that learning from "explanation traces" in a progressive manner allows smaller models to imitate the reasoning processes of larger foundation models. Furthermore, in mathematical and logical reasoning tasks, CL has been utilized to transition models from simple single-step problems to multi-step reasoning chains, significantly mitigating the difficulty of solving complex problems directly (Luo et al., 2025).

### A.1.3 Interpretability in LLM Reasoning

The interpretation of reasoning in Large Language Models (LLMs) has evolved from analyzing surface-level generations to probing the internal causal mechanisms that drive them (Zhao et al., 2024a,b; Wang et al., 2024b).

A natural starting point for interpretability is to treat generated explanations—most prominently CoT—as a proxy for the model’s decision-making process (Wei et al., 2022). However, recent scholarship challenges this assumption, characterizing CoT as often unfaithful. Evidence suggests that intermediate reasoning steps can be post-hoc rationalizations that do not causally determine the final prediction (Turpin et al., 2023), and increasing reasoning burden does not necessarily equate to computational transparency (Lanham et al., 2023; Arcuschin et al., 2025; Jin et al., 2025a). Consequently, the field has shifted focus from verifying *plausible explanations* to establishing *causal accounts* of model behavior.

To bridge the gap between model inputs and outputs, mechanistic interpretability develops tools that aim to isolate components that are necessary and sufficient for particular behaviors, and to characterize how information is represented and transformed across the network (Wang et al., 2022; Gantla, 2025). A prominent line of work uses causal interventions: most notably, causal tracing and activation patching to perform controlled swaps between activations induced by “clean” versus “corrupted” inputs, thereby localizing where task-relevant signals reside and empirically testing how those signals propagate through layers and attention pathways (Wang et al., 2022; Zhao et al., 2025; Meng et al., 2022; Jin et al., 2025c). Complementary approaches focus less on direct causal disruption and more on interpretability via readouts: representation-decoding frameworks such as Patchscopes map hidden states into structured textual probes, offering a unified interface for inspecting intermediate computations under a variety of intervention patterns (Ghandeharioun et al., 2024). Related “lens” methods, including the Logit Lens, project intermediate activations into the vocabulary (logit) space to track how candidate outputs become linearly recoverable across depth; while

lightweight and often used diagnostically, these readouts are frequently most informative when paired with causal tests that distinguish genuine computation from superficial decodability (nostalgebraist, 2020; Wendler et al., 2024; Geva et al., 2021; Belrose et al., 2023).

At a finer level of analysis, mechanistic interpretability work tries to break down a model’s behavior into concrete computational pathways (“circuits”) and smaller features that can be followed as they appear and change across different inputs (Elhage et al., 2021, 2022). A central thread in this direction explains in-context learning through specific attention-head motifs: most notably induction heads that appear to implement a concrete pattern-copying mechanism (Olsson et al., 2022). To move beyond correlational stories, subsequent work has introduced more stringent validation procedures, such as causal scrubbing and automated circuit discovery (ACDC), which use behavior-preserving resampling and controlled interventions to test whether a proposed circuit is genuinely explanatory rather than an artifact of spurious co-activation (Conmy et al., 2023).

In parallel, feature-centric approaches address the pervasive polysemanticity of dense activations by learning sparse decompositions: Sparse Autoencoders (SAEs) attempt to “unsuperpose” representations into more interpretable directions that are often closer to monosemantic features, enabling a complementary level of analysis that is not limited to predefined motifs like individual heads (Huben et al., 2024; Bricken et al., 2023; He et al., 2025; Han et al., 2025).

Overall, the literature increasingly reflects a convergence in methodology, pairing explanatory narratives with rigorous causal tests and feature-level decomposition in order to debug and interpret reasoning processes in modern LLMs.

#### A.1.4 Learning Dynamics

A complementary line of work studies how optimization shapes representations over the course of training. Classical results on the *implicit bias* of gradient-based optimization show that, even without explicit regularization, gradient descent on separable classification problems converges in direction to max-margin solutions, linking training dynamics to margin growth and norm evolution (Soudry et al., 2018; Ji and Telgarsky, 2019); related analyses extend these behaviors to stochastic gradient descent (Nacson et al., 2019).

More recently, phase-transition-like learning phenomena such as *grokking* highlight that models can move from memorization to generalization late in training, motivating mechanistic accounts in terms of regime changes in training dynamics and feature learning (Kumar et al., 2024; DeMoss et al., 2025). Complementary to this line, (Ren and Sutherland, 2025) propose a learning-dynamics framework for *LLM fine-tuning* (including SFT and preference optimization), characterizing how learning on specific examples influences predictions on others and using this lens to explain several counter-intuitive fine-tuning behaviors. These perspectives motivate using simple representation-level statistics (e.g., norms, energy concentration) as probes of how effective features are selected and amplified throughout training.

## A.2 All Metrics

### A.2.1 Sparsity Metrics

We analyze the sparsity of the activation vector  $\mathbf{h} \in \mathbb{R}^d$  extracted from the last hidden state of the model. Since raw activations are rarely absolute zeros in floating-point representations, we utilize these metrics that capture the *effective sparsity* (i.e., the peakedness of the distribution).

**Hoyer Sparsity.** Derived from the relationship between the  $\ell_1$  and  $\ell_2$  Norms, Hoyer sparsity measures how close a vector is to being sparse (containing mostly zeros). For an activation vector  $\mathbf{h}$  of dimension  $d$ :

$$\text{Hoyer}(\mathbf{h}) = \frac{\sqrt{d} - \frac{\|\mathbf{h}\|_1}{\|\mathbf{h}\|_2}}{\sqrt{d} - 1} \quad (\text{A.1})$$

where  $\|\mathbf{h}\|_1$  is the  $\ell_1$  norm and  $\|\mathbf{h}\|_2$  is the spectral norm. A value of  $\mathbf{0}$  indicates a dense, uniform vector ( $h_i = c, \forall i$ ) and a value of  $\mathbf{1}$  indicates maximum sparsity (only one component is non-zero).

**Gini Index.** Originally used in economics to measure income inequality, the Gini index here quantifies the inequality of neural activation strengths. High inequality implies that a few neurons dominate the representation while the majority remain suppressed (sparse).

$$\text{Gini}(\mathbf{h}) = \frac{\sum_{i=1}^d (2i - d - 1) |h_{(i)}|}{d \sum_{i=1}^d |h_{(i)}|} \quad (\text{A.2})$$

where  $|h_{(1)}| \leq |h_{(2)}| \leq \dots \leq |h_{(d)}|$  are the sorted absolute values of the activations. A higher Gini index correlates with a sparser representation.

**Effective Rank.** Effective rank quantifies how concentrated the activation energy is across dimensions. Given  $\mathbf{h} \in \mathbb{R}^d$ , define a distribution over dimensions by

$$p_i = \frac{h_i^2}{\sum_{j=1}^d h_j^2}, \quad i = 1, \dots, d, \quad (\text{A.3})$$

and entropy  $H(\mathbf{p}) = -\sum_{i=1}^d p_i \log(p_i + \epsilon)$ . We then compute

$$\text{EffRank}(\mathbf{h}) = \frac{\exp(H(\mathbf{p}))}{d} \in (0, 1]. \quad (\text{A.4})$$

Larger values indicate more evenly spread energy (denser representations), while smaller values indicate stronger concentration on a few dimensions (sparser representations).

## A.2.2 Model Parameter Metrics

We validate our findings across a range of transformer model sizes, ranging from 0.3M to 1.3B parameters, using the Llama architecture, we need to know how to compute the model Parameter size  $N_{params}$ . As detailed in [Table 1](#), the model complexity is controlled by the hidden size ( $d_{model}$ ), the intermediate MLP size ( $d_{mlp}$ ), the number of attention heads ( $H$ ), and the network depth ( $L$ ). Assuming a standard Llama-based architecture (utilizing SwiGLU activation and Rotary Embeddings), the approximate parameter count  $N_{params}$  for the non-embedding layers is calculated as:

$$N_{params} \approx L \cdot \left( \underbrace{4d_{model}^2}_{\text{Attention}} + \underbrace{3d_{model} \cdot d_{mlp}}_{\text{FeedForward (SwiGLU)}} \right) \quad (\text{A.5})$$

where the attention block consists of  $W_Q, W_K, W_V, W_O$ , contributing  $4d_{model}^2$ . The FeedForward block (SwiGLU) involves three projections (gate, up, down), contributing  $3d_{model} \cdot d_{mlp}$ .

[Figure 8](#) summarizes how  $L$  (layers) and  $H$  (attention heads) scale with model size in our Llama sweep. Both increase in discrete steps as the parameter count grows.

Model Depth & Attention Heads Scaling

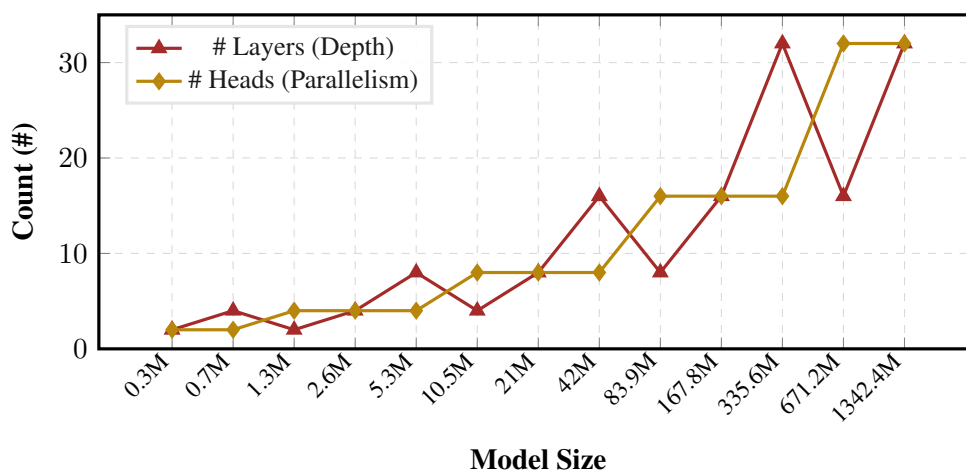


Figure 8: Scaling of computational depth (Layers) and parallel attention capacities (Heads) across Llama models. Both metrics show a step-wise increase consistent with the model’s total parameter growth.

### A.3 Reasoning Prompt

The following demonstrates the implicit reasoning prompts designed to address knowledge conflicts, mathematical reasoning, and multiple-choice questions, and related tasks:

#### Example Reasoning Prompt 1

**System:** You are a helpful assistant. For each multiple choice question, you must answer with ONLY a single letter: A, B, C, D... Do not explain or add any other text.

**User:** {prompt\_text}. Answer the question with only the letter:

#### Example Reasoning Prompt 2

**System:** You are a helpful Knowledge Conflict assistant. You should judge the knowledge in the sentence is correct or not. You should answer with ONLY a single letter: True or False. Do not explain or add any other text.

**User:** {prompt\_text}. Answer the question with only the letter:

#### Example Reasoning Prompt 3

**System:** You are a helpful math assistant. Provide the final answer in the end.

**User:** {prompt\_text}. Please provide the final answer in the end.

#### Knowledge Conflict Dataset Entry 1

**Main Entity:** Variable

**Conflict Method:** Shuffling (Variable  $\rightarrow$  Random variable)

---

**Parametric Knowledge (Ground Truth):**

In programming, a variable is a named container that stores a value. It can hold different data types, such as numbers or strings, and its value can be changed during the execution of a program.

**Conflicting Knowledge (Injected Noise):**

In programming, a **Random variable** is a named container that stores a value. It can hold different data types, such as numbers or strings, and its value can be changed during the execution of a program.

---

**Generated Questions:** What is a named container that stores a value and can be changed during the execution of a program?

#### Knowledge Conflict Dataset Entry 2

**Main Entity:** Equation

**Conflict Method:** Substitution (two  $\rightarrow$  9)

---

**Parametric Knowledge (Ground Truth):**

An equation is a mathematical statement that shows the equality of **two** expressions. It typically consists of variables, constants, and mathematical operations.

**Conflicting Knowledge (Injected Noise):**

An equation is a mathematical statement that shows the equality of **9** expressions. It typically consists of variables, constants, and mathematical operations.

---

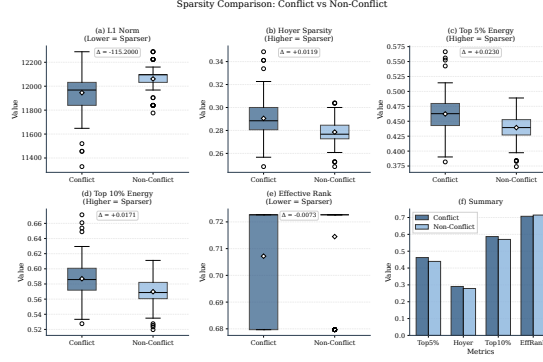
**Generated Questions:** How many expressions does an equation typically show the equality of?

## A.4 More Details about Knowledge Conflict and different types of In-context Learning

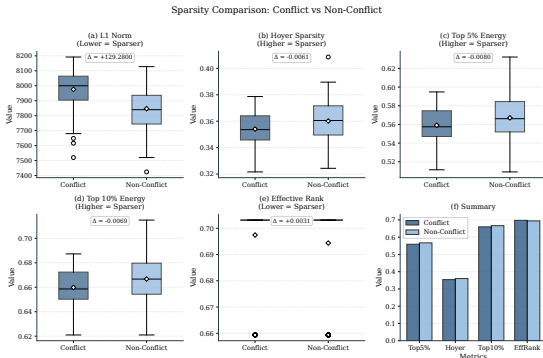
### A.4.1 Details about Knowledge Conflict Dataset

This dataset Wang et al. (2024b) operates on a *Knowledge Injection and Interference* logic through a two-step process. First, it establishes Parametric Knowledge by defining ground-truth facts the model acquired during pre-training, such as the standard definition of a programming variable. Second, it performs Conflict Generation using a “shuffling” method, where the core entity is replaced with a phonetically or conceptually similar but semantically distinct term (e.g., substituting *variable* with *random variable*). This creates a strategic contradiction between the provided context and the model’s internal common sense.

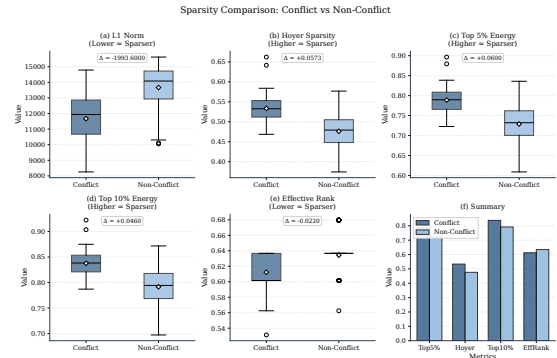
This dataset is particularly suitable for our research because it allows for the precise control of Out-of-Distribution (OOD) intensity by manipulating the degree of external knowledge conflict. As we posit that adversarial distractors can transform an original “easy” input into a “conflict” perturbed variant, this framework provides a quantifiable way to increase task difficulty. By introducing these specific knowledge conflicts as distractor items, we can systematically simulate OOD scenarios where the model’s internal parametric memory directly clashes with contradictory external evidence.



(a) Llama3.1-70B



(b) Qwen2.5-32B



(c) Qwen2.5-70B

Figure 9: **Sparsity analysis across different models.** (a) Visualizes the sparsity pattern of Llama3.1-70B. (b) and (c) compare the Qwen2.5 series models (32B and 70B).

#### A.4.2 More Results on Larger Model

To verify the universality of our hypothesis that OOD samples trigger higher activation sparsity in the last hidden layer, we extended our evaluation to a diverse set of large-scale foundation models and used the same knowledge conflict dataset as Wang et al. (2024b). Specifically, we selected models varying in both architecture and parameter size, including Qwen2.5-32B, Qwen2.5-70B, and Llama-3.1-70B.

As illustrated in Figure 9, the experimental results are highly consistent across all tested models. We observe that samples involving knowledge conflicts (a representative form of OOD data) systematically induce significantly sparser activation patterns compared to consistent (in-distribution) samples. This phenomenon remains robust regardless of the model’s scaling or architectural design. For instance, even in the 70B parameter language models, the activation density drops sharply when the model encounters conflicting information. These findings strongly corroborate our core conclusion: activation sparsity serves as an architecture-agnostic proxy for sample difficulty and OOD status, validating the effectiveness of using sparsity for data ranking.

Context Setting	Context Prompt	Query Prompt	🙄	😊
Related	On the inside, bananas are white.	What color are mangoes on the inside? They are	white	orange
Irrelevant	The capital of Canada is Ottawa.	What color are mangoes on the inside? They are	Ottawa	orange
Random	Promotion	What color are mangoes on the inside? They are	Promotion	orange
<i>Distraction over Counterfactual Context</i>			🐾	😊
Counterfactual	On the inside, bananas are green.	What color are mangoes on the inside? They are	green	white

Table 2: Prompt Setup (Niu et al., 2025). We follow the exact same prompt setup as Niu et al. (2025). The emojis represent the target tokens: 🐾: counterfactual; 🙄: distracting; 😊: correct.

### A.4.3 Different Kind of In-Context Learning

Following the experimental framework established by Niu et al. (2025), we devised multiple In-Context Learning (ICL) strategies to comprehensively evaluate the model’s reasoning capabilities under different prompting conditions. Specifically, we implemented four distinct prompting variants, taken from Niu et al. (2025), as shown in Table 2.

Context Setting	$L_1$ Norm	Top-5% Energy	Top-10% Energy	Eff. Rank
Related	5066.96	0.5723	0.6715	0.6715
Irrelevant	5072.15	0.5816	0.6772	0.6764
Random	3689.13	0.7600	0.8203	0.5987
Counterfactual	4938.74	0.5978	0.6937	0.6680

Table 3: Sparsity metrics averaged over samples across different context settings in Qwen2.5-1.5B.

We categorize these prompting strategies into two primary dimensions: *Contextual Distraction* and *Counterfactual Conflict*. In settings of Contextual Distraction: comprising Related, Irrelevant, and Random contexts, the input provides truthful but potentially noisy information, aiming to measure the model’s susceptibility to blindly copying context tokens versus accessing its internal parametric knowledge (😊). Specifically, the ‘Related’ context tests the capability to distinguish between semantically similar attributes within a domain, whereas ‘Irrelevant’ and ‘Random’ contexts serve as baselines to assess the model’s resilience against pure recency bias and token repetition. Conversely, the Counterfactual Conflict setting introduces a direct contradiction between the context and ground truth, creating a tripartite competition in the probability space. Following this categorization, we further investigated the sparsity patterns of the model’s last hidden state representations under these distinct settings as Table 3 shows.

Our results provide empirical support for the hypothesis that inputs deviating further from the pre-training distribution (OOD) induce higher activation sparsity. We observe a clear gradient of sparsity corresponding to the degree of distribution shift. These metrics collectively validate that sparsity is positively correlated with the OOD nature of the input. As the context shifts from natural language (Related) to semantic conflict (Counterfactual) and finally to complete noise (Random), the model’s last hidden state representations become increasingly sparse and low-rank.

As shown in Table 3, our results provide empirical support for the hypothesis that inputs deviating further

from the pre-training distribution (OOD) induce higher activation sparsity. The Random setting, representing the most severe OOD scenario characterized by semantic and structural noise, exhibits distinct hyper-sparsity characteristics. It records the lowest activation magnitude ( $L_1 \approx 3689.13$ ) while simultaneously showing the highest energy concentration (Top-5% Energy  $\approx 0.7600$ ), indicating that nonsensical inputs fail to activate broad semantic circuits, thereby concentrating signal flow into a narrow subset of neurons and collapsing the representation into a lower-dimensional subspace as evidenced by the significantly lower Effective Rank (0.5987). A more subtle trend is observed when comparing Counterfactual to Related contexts; although both are grammatically well-formed, the semantic conflict in the Counterfactual setting induces slightly higher sparsity than Related inputs ( $L_1$ : 4938.74 < 5066.96; Top-5% Energy: 0.5978 > 0.5723). This suggests that processing “lies” or counter-knowledge conflicts engages fewer knowledge retrieval circuits compared to processing truthful, coherent information, effectively “pruning” the activation of conflicting parametric knowledge. Conversely, the Related and Irrelevant settings serve as in-distribution baselines, showing the highest  $L_1$  norms and lowest energy concentrations, which reflect a dense, broad activation of the model’s semantic networks in response to natural linguistic structures.

## A.5 More Details about MMLU-Robust

### A.5.1 Example in MMLU-PRO and MMLU-Robust

MMLU-Pro (Wang et al., 2024c) is an enhanced version of the original Massive Multitask Language Understanding (MMLU) benchmark (Hendrycks et al., 2021), developed to address shortcomings that have emerged as modern LLMs have improved. In particular, the original MMLU has become increasingly *too easy* for state-of-the-art models and is affected by data noise in certain subsets. MMLU-Pro introduces several key improvements over its predecessor. ♦ **Increased difficulty.** Overly simple factual questions are filtered out and replaced with more challenging problems that require multi-step and rigorous reasoning. ♦ **Expanded answer space.** The number of multiple-choice options is increased from four to ten, substantially reducing the likelihood of correct answers due to random guessing and better reflecting genuine reasoning ability. ♦ **Broader coverage.** The benchmark comprises over 12,000 questions across 14 core academic domains, spanning STEM, humanities, and social sciences.

To systematically evaluate the last hidden state under progressively intensifying OOD conditions, we construct a variant dataset, **MMLU-Robust**. Building on the already challenging MMLU-Pro benchmark, which features ten multiple-choice options, we introduce an iterative distractor augmentation mechanism. The idea is simple: adding more plausible options makes the task harder. We borrow some ideas from the robust attack of LLM Zhou et al. (2024); Zhang et al. (2024b,a)

In particular, we employ a perturbation function  $\mathcal{P}(\cdot)$  to generate plausible but incorrect distractors derived from the existing option set. For a given question with an initial option set  $\mathcal{O}_{10}$  ( $|\mathcal{O}_{10}| = 10$ ), we select a subset of non-ground-truth options and apply semantic or numerical perturbations (e.g., sign flipping, unit alteration, or logical inversion) to create new adversarial options. These perturbed variants are injected back into the pool to form expanded sets  $\mathcal{O}_{15}$  and  $\mathcal{O}_{20}$ .

This process creates a controlled “interference gradient.” By increasing the option count from 10 to 15 and finally to 20, we densify the solution space with highly correlated noise, forcing the model to discern increasingly subtle differences. We hypothesize that this artificially induced complexity acts as a proxy for severe OOD shifts, triggering the sparse representation mechanism described in our main findings.

### MMLU-Pro Dataset Samples

#### Sample 1: Number Theory

**Question:** Let  $A$  be the set of all ordered pairs of integers  $(m, n)$  such that  $7m + 12n = 22$ . What is the greatest negative number in the set  $B = \{m + n : (m, n) \in A\}$ ?

**Options:**

- (A) -5 (B) 0 (C) -3  
(D) -7  
(E) **-4** (Correct) (F) -6  
(G) -1 (H) -2 (I) -9 (J) N/A

**[CoT Reasoning]** We have  $12n = 22 - 7m$ . A particular solution is  $m = -2, n = 3$ , so  $m + n = 1$ . The general solution is  $m = -2 + 12k, n = 3 - 7k$ . Then  $m + n = 1 + 5k$ . For  $m + n < 0$ , we need  $5k < -1$ , so  $k \leq -1$ . Max value is at  $k = -1$ :  $1 + 5(-1) = -4$ .

### MMLU-Robust Dataset Samples

#### Sample 1: Number Theory

**Question:** Let  $A$  be the set of all ordered pairs of integers  $(m, n)$  such that  $7m + 12n = 22$ . What is the greatest negative number in the set  $B = \{m + n : (m, n) \in A\}$ ?

**Options:**

- (A) -5 (B) 0 (C) -3  
(D) -7  
(E) **-4** (Correct) (F) -6  
(G) -1 (H) -2 (I) -9 (J) N/A  
(H) **1** [Valid member, but positive]  
(I) **-14** [Valid member, but  $< -4$ ]  
(J) **4** [Sign flip]  
(K) **-8** [Dense noise]  
(M) **125** [Dense noise]

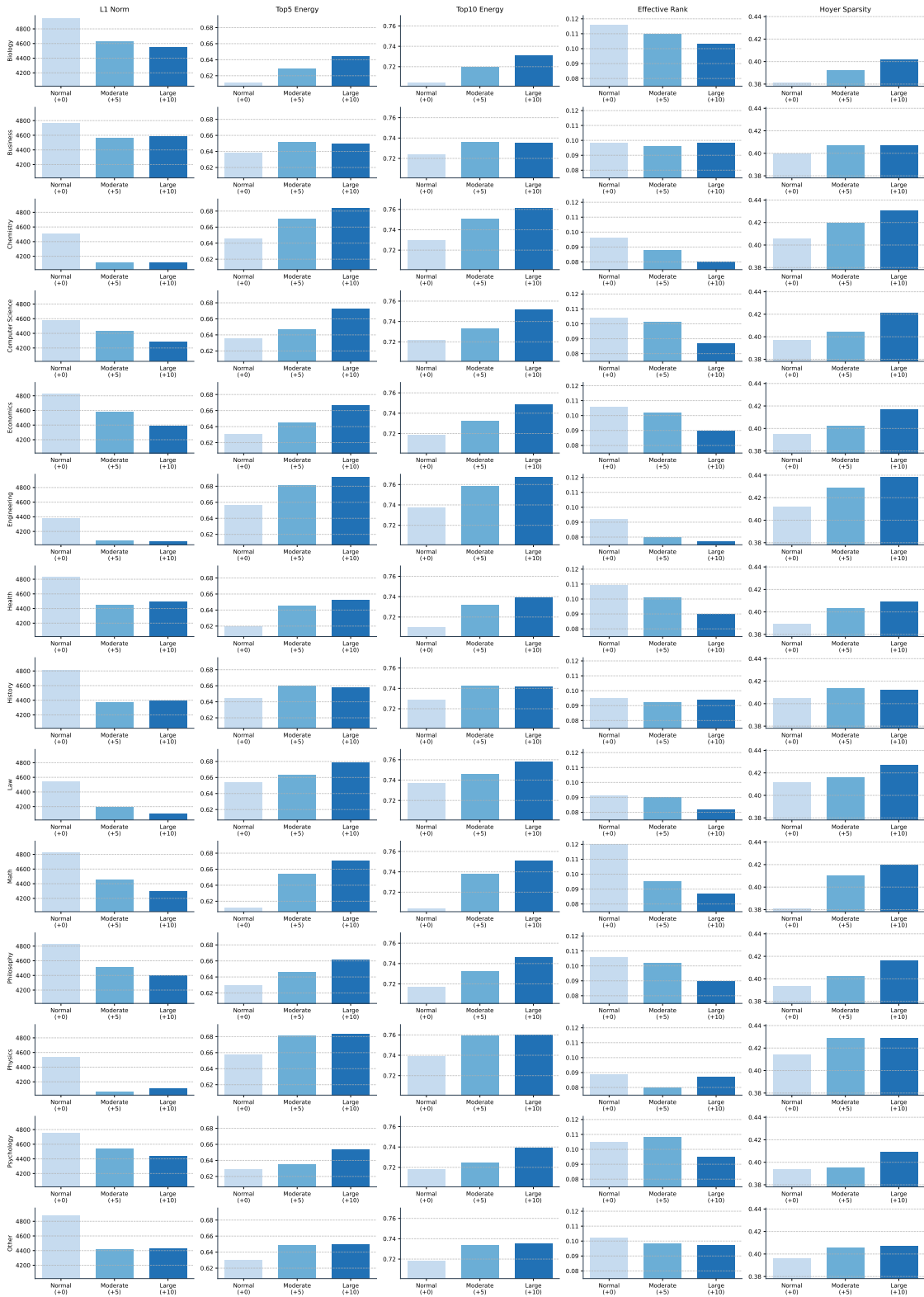
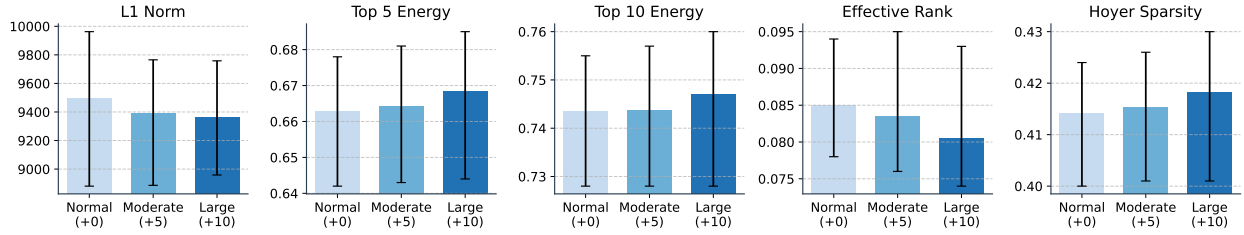
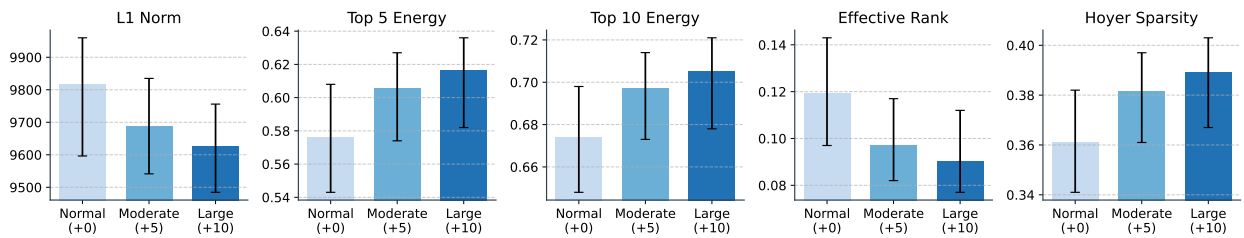


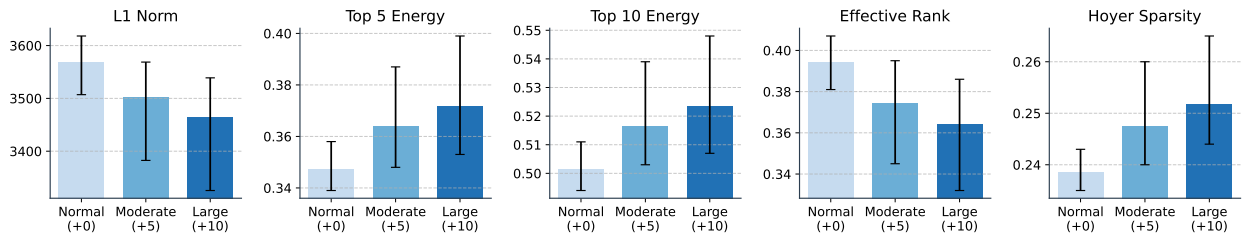
Figure 10: Per-domain sparsity statistics for Qwen2.5-3B-Instruct on MMLU-Robust.



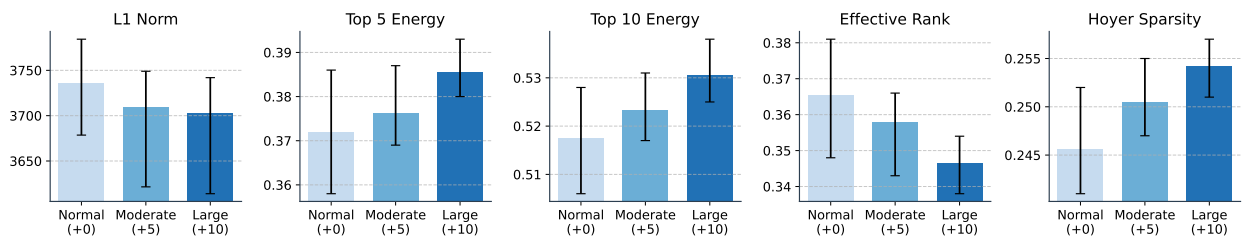
(a) **Qwen2.5-7B-Instruct**



(b) **Qwen2.5-14B-Instruct**



(c) **Llama-3.2-1B-Instruct**



(d) **Llama-3.2-3B-Instruct**

Figure 11: Average sparsity statistics on MMLU-Robust for more LMs.

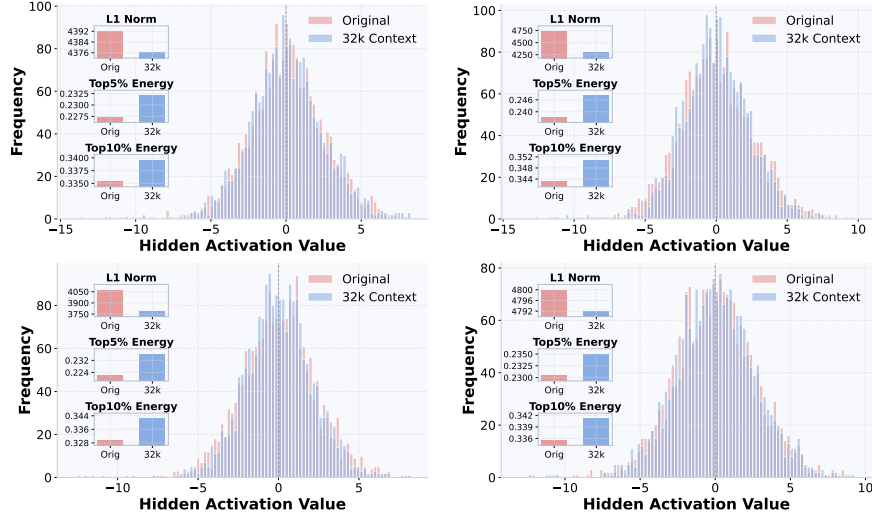


Figure 12: **Task complexity induces sparsity.** Representation activation showing increased sparsity in harder tasks (32k context, blue) compared to original settings (Short context, red). Three metrics consistently demonstrate higher sparsity for challenging inputs.

### A.5.2 More Results in MMLU-Robust

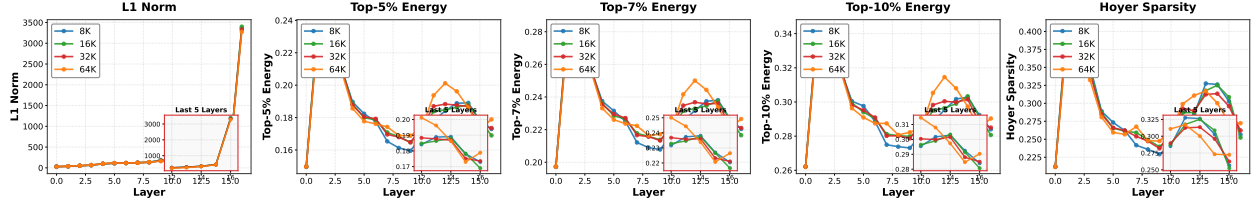
Figure 10 reports a fine-grained breakdown of sparsity-related results on MMLU-Robust for **Qwen2.5-3B-Instruct**, grouped by academic area and evaluated under three adversarial noise levels (Normal (+0) / Moderate (+5) / Hard (+10)). For each area, we aggregate the last hidden state statistics across questions and visualize five metrics: normalized  $\ell_1$  magnitude, Top-5% Energy, Top-10% Energy, Effective Rank, and Hoyer Sparsity.

Figure 11 reports averaged results for four additional LMs. Across these models, we observe the same qualitative pattern as in the main results: increasing OOD difficulty consistently leads to sharper sparsity in the last hidden state across domains and metrics. This consistency suggests that the observed behavior is not specific to a particular model size or architecture. We encourage readers to reproduce and extend our analysis on additional models, datasets, and evaluation settings to further test the generality of this phenomenon.

To address the space limitation in the main text, we further report a per-area analysis on MMLU(-Robust/MMLU-Pro), where we evaluate each academic field separately to verify whether the sparsity–difficulty relationship holds beyond overall averages. As shown in Figure 10, the trend remains robust across domains: as adversarial noise increases (Normal  $\rightarrow$  Moderate  $\rightarrow$  Hard), the representation becomes consistently *more sparse* in nearly every area. Concretely, harder (more perturbed) inputs exhibit lower normalized  $\ell_1$  magnitude and effective rank, together with higher Top- $k$  energy concentration and Hoyer sparsity. While the absolute metric levels vary by subject, the direction of change is highly consistent, supporting the conclusion that the “harder-is-sparser” phenomenon is not driven by a small subset of domains but persists broadly across academic areas.

### A.6 Long Context Reasoning Details

To further probe whether our “harder-is-sparser” finding extends beyond adversarial perturbations, we study a *long-context reasoning* setting where difficulty is increased by expanding the background context length. Concretely, we compare short-context prompts against a long-context (32K) variant constructed



CONTEXT: Sparsity metrics across all layers for Llama3.2-1B under varying context lengths (8K, 16K, 32K, 64K).

Figure 13: **Layer-wise Sparsity across Context Lengths.** While intermediate layers show minimal variation across contexts, the final layers exhibit sharp divergence: longer contexts consistently produce sparser representations. This experiment was done at LongReasonQA (Li et al., 2025a), which can control the background context length.

from LongReasonQA, which controls the amount of background evidence while keeping the core question unchanged. This setup isolates the effect of contextual complexity (more tokens, more distractors, and longer-range dependency) on internal representations.

Figure 12 visualizes the distribution of last-layer activations under short vs. 32K context. The long-context condition exhibits a visibly more concentrated distribution, and the accompanying sparsity metrics shift consistently in the “sparser” direction: the normalized  $\ell_1$  magnitude decreases, while Top- $k$  energy concentration increases. These results mirror the robustness experiments in the main text, suggesting that increasing task complexity via longer contexts induce a sharper, more selective representation at inference time.

We further examine *where* this sparsification emerges along the depth of LLM. Figure 13 reports layer-wise sparsity metrics for **Llama-3.2-1B-Instruct** across 8K/16K/32K/64K contexts. A clear pattern appears: intermediate layers remain largely stable across context lengths, whereas the final layers diverge sharply, with longer contexts producing consistently sparser activations (lower  $\ell_1$  Norm and effective-rank, higher Top- $k$  energy and Hoyer sparsity). This localization to late layers supports the view that long-context difficulty primarily changes the *final-stage computation* that consolidates evidence into the prediction-relevant subspace, rather than uniformly reshaping representations throughout the entire LLM.

LongReasonQA (Li et al., 2025a) is a long-context reasoning benchmark that systematically controls the amount of background context (e.g., 8K/16K/32K/64K) while keeping the core question and answer format fixed, enabling a clean test of how increasing context length affects model reasoning and internal representations as Figure 14.

## A.7 Pretraining data construction details

### A.7.1 Model and training setup.

We train a randomly initialized, decoder-only Transformer following the LLaMA architecture. Given a configuration llama- $L$ - $H$ , we set the hidden size to  $d = 64H$ , the number of layers to  $L$ , the number of attention heads to  $H$ , and the MLP intermediate size to  $2d$ . The model is trained with a lightweight character-level tokenizer whose vocabulary consists of :{Q, P, 0–9, space, newline, ‘-’, ‘?’}, <BOS>, <EOS>, <PAD>, <UNK>}. Training data are generated from a latent-rule knowledge graph; each sample is a single triple serialized as “Q{h} P{r} Q{t}\n” and optimized with the standard next-token prediction objective (labels identical to inputs, with padding labels masked by  $-100$ ). We use the HuggingFace Trainer with per-device batch size 32, learning rate  $10^{-4}$ , cosine learning-rate schedule, warmup ratio 0.2, and no

### LongReason (8K) example (truncated background)

**Background (truncated):**

Following the destruction of the house and its contents, Parks filed an insurance claim ...

⋮

... Understanding this ejection process is essential for comprehending how “Omega” achieves its propulsion objectives.

**Question:**

In the context of space station “Omega,” what does “these fluids” refer to?

**Choices:**

(A) Wave modulator (B) Ion converter (C) Pulsed high-energy currents (D) Ion streams

**Gold answer:** (D)

Figure 14: **A LongReason 8K instance.** We show one example used in our long-context evaluation. For readability, the background is truncated (head + tail); the full context is available in the dataset.

weight decay. Unless otherwise specified, we train for `max_steps` steps (with optional BF16) and save a single checkpoint at the end of training.

#### A.7.2 Synthetic knowledge graph generation.

We construct a synthetic knowledge graph (KG), rather than a real-world one, because we can control the graph’s size and complexity. By coupling a latent rule set with a graph growth process, we follow the setting of Wang et al. (2025b). We first sample a collection of acyclic relational rules, where each rule is represented as a relation chain  $(r_0 \Leftarrow r_1, \dots, r_\ell)$  with  $\ell \in [L_{\min}, L_{\max}]$ . Next, we instantiate these rules on fresh entity nodes to form an initial backbone graph: for each rule, we create a directed path following the body relations  $(r_1, \dots, r_\ell)$  and additionally insert the implied head edge  $r_0$  between the same endpoints. After building the initial backbone graph, we grow it to the desired size by adding one new entity at a time. For each new entity, we create  $m$  connections to existing entities. The relation type of each new connection is not chosen completely at random; instead, it is restricted by a relation-adjacency map that records which relations tend to appear together in the sampled rules. Optionally, we bias the attachment toward already well-connected entities, producing a power-law degree distribution.

To inject deductive structure, we periodically apply a subset of rules to existing nodes via stochastic traversal. For each candidate head entity, we follow the rule body edges on the current graph (with probability  $p_{\text{mcmc}}$  at each hop) to obtain reachable tail entities; whenever a rule fires, we add the implied triple  $(h, r_0, t)$  and record its supporting rule(s). We refer to such implied edges as *deductible* triples, while the remaining edges are treated as *atomic* triples. We then form the training set as a mixture of atomic and deductible triples controlled by a deductible ratio  $\rho$  and remove all non-training edges from the graph to prevent leakage. Finally, we design three evaluation splits: an in-distribution (ID) set sampled from the training triples (measuring memorization), and two out-of-distribution (OOD) sets composed of deductible triples stratified by their shortest supporting rule length, resulting in long-path and short-path OOD tests. Short-path OOD contains deductible triples whose shortest supporting rule is only 1–2 steps, while long-path OOD requires at least 3 steps. In our experiments, the short path is consistently harder than the long path. The key reason is

### LongReason (8K) example (paraphrased & truncated)

**Background (paraphrased, truncated):**

Note that adblockers might block our captcha, and other functionality on BHW so if you don't see the captcha or see reduced functionality please disable adblockers to ensure full functionality, note we only allow relevant management verified ads on BHW.

:

Briner's observations confirm creationist Ice Age studies. It is most reasonable, given the Bible's history, that there was a single Ice Age, and that the largest extent of ice lasted for only hundreds of years, beginning around 2400 BC. It is possible that the period of time wherein the "lion's share" of melting apparently occurred was the only time that it occurred. The remaining thousands of years would therefore be a product not of data, but of the assumption of deep time.

**Question:**

Which of the following, if true, does not weaken the viewpoint about the restoration of the jade pine forest in the country of Novaland after a chemical spill?

**Choices:**

- (A) The pollution in the forest may have reduced to a level where some trees can survive.
- (B) Apart from artificially planted species, wild plants have also appeared.
- (C) Certain specific pollutants have been removed, but the heavy metal content in the forest soil is still higher than before.
- (D) The types and numbers of birds appearing in the forest are still very few, not reaching the scale before the pollution.

**Gold answer:** (B)

Figure 15: A LongReason 8K instance (paraphrased). We follow the same presentation format as our long-context example: truncated background + multiple-choice inquiry + gold label.

that, under our synthetic generator, short rules are typically *broad* while long rules are more *selective*. For OOD-SHORT, the rule body is easy to satisfy, so the same query  $(h, r)$  often admits multiple deducible tails (i.e., several  $t$ 's are consistent with the rules and the current graph), creating substantial ambiguity and stronger competition among plausible answers. In contrast, OOD-LONG imposes stricter compositional constraints, so far fewer paths match the full chain, and the set of valid deducible tails is usually much smaller (often close to a unique solution). As a result, the long-path split is easier, whereas the short-path split is harder in our setting. The structure of the knowledge graph construction can be found in [Table 4](#).

## A.8 An Extended Discussion and Future Work

Our investigation establishes a robust empirical law: *The farther the distribution shift, the sparser the representation*. Beyond the raw observations, this section synthesizes the underlying mechanisms and the broader implications of this phenomenon.

We hypothesize that explicitly training for "OOD-like" sparsity could improve model robustness and generalization, effectively simulating the "active suppression" mechanism during the learning phase. Our experiments utilized dense architectures (Llama series). Mixture-of-Experts (MoE) models introduce structural sparsity by design. Investigating whether the "OOD-induced sparsity" phenomenon persists in MoE architectures, or if the routing mechanism absorbs the shift would be critical for generalizing our findings to the next generation of sparse foundation models. Our study focused on reasoning tasks where the model

Stage	Synthetic KG construction (as implemented)
<b>Universe</b>	Entities are symbolic nodes $Q_0, Q_1, \dots, Q_{n-1}$ ; relations are $P_0, P_1, \dots, P_{n_r-1}$ .
<b>Rule sampling</b>	Sample a pool of candidate rules as relation chains: $(r_0 \Leftarrow r_1, r_2, \dots, r_\ell)$ with $\ell \in [L_{\min}, L_{\max}]$ . Optionally apply length-weighted sampling with temperature $\tau$ (shorter rules sampled more often). Acyclicity is enforced via a dependency graph over relations.
<b>Backbone graph initialization</b>	Construct an initial directed multigraph by instantiating each sampled rule on fresh entity nodes: create a path $Q \xrightarrow{r_1} \dots \xrightarrow{r_\ell} Q'$ and add the implied edge $Q \xrightarrow{r_0} Q'$ . Maintain per-relation entity pools (“repeated entities”) for later attachment.
<b>Graph growth (structural prior)</b>	Iteratively add new nodes until reaching $n$ entities. Each new node attaches $m$ edges by sampling relations constrained by an adjacency map derived from rule co-occurrence (also supporting a power-law attachment mode).
<b>Deductible edge injection</b>	Periodically enumerate candidate heads $h$ and attempt to apply a subset of rules (“deductible rules”) by stochastic traversal: follow each rule body with probability $p_{\text{mcmc}}$ to obtain reachable tails $t$ ; if successful, add the implied triple $(h, r_0, t)$ as a <i>deductible</i> edge and record its supporting rule(s).
<b>Train graph pruning</b>	Form training triples as a mixture of <i>atomic</i> edges (not derivable) and <i>deductible</i> edges (derivable), controlled by deductible ratio $\rho$ . All edges not selected for training are removed from the graph to avoid leakage.
<b>Test set design (difficulty)</b>	Three evaluation splits are constructed: (i) <b>ID/Easy</b> : sampled directly from training triples (memory); (ii) <b>OOD-Long/Medium</b> : deductible triples supported by <i>long</i> rules (e.g., $\geq 3$ steps); (iii) <b>OOD-Short/Hard</b> : deductible triples supported by <i>short</i> rules (e.g., 1–2 steps). For OOD splits, “seen tails” are collected from alternative deductive paths for harder negative sampling.
<b>Text serialization</b>	Each triple is serialized as a character-level sequence: $Q\{h\} P\{r\} Q\{t\}$ (plus newline), enabling a lightweight tokenizer and controlled vocabulary.

Table 4: Synthetic knowledge graph generation via a latent-rule process: rule sampling, graph growth, deductible edge injection, and difficulty-controlled evaluation splits.

generally attempts to solve the problem. An intriguing direction is to analyze sparsity patterns during hallucinations. Does a model exhibit *low* sparsity (high confidence/confusion) when it hallucinates, or does it exhibit *extreme* sparsity (information collapse)? Establishing a correlation between sparsity signatures and factual errors could lead to lightweight, white-box hallucination detection methods that do not require external fact-checking.